Evaluation and application of a fine-resolution global data set in a semiarid mesoscale river basin with a distributed biosphere...

Article *in* Journal of Geophysical Research Atmospheres · November 2011

DOI: 10.1029/2011JD015990

CITATIONS
38

READS
128

7 authors, including:

Fuxing Wang
Le Laboratoire de Météorologie Dynamique (L...
7 PUBLICATIONS **88** CITATIONS
SEE PROFILE

Huicheng Zhou
Dalian University of Technology
88 PUBLICATIONS **536** CITATIONS
SEE PROFILE

Kun Yang
Chinese Academy of Sciences
146 PUBLICATIONS **4,165** CITATIONS
SEE PROFILE

Aihui Wang
Chinese Academy of Sciences
24 PUBLICATIONS **850** CITATIONS
SEE PROFILE

Evaluation and application of a fine-resolution global data set in a semiarid mesoscale river basin with a distributed biosphere hydrological model

Fuxing Wang,[1,2] Lei Wang,[2,3] Toshio Koike,[2] Huicheng Zhou,[1] Kun Yang,[3] Aihui Wang,[4] and Wenlong Li[5]

Received 24 March 2011; revised 12 September 2011; accepted 12 September 2011; published 10 November 2011.

[1] Accurate estimates of basin-wide water and energy cycles are essential for improving the integrated water resources management (IWRM), especially for relatively dry conditions. This study aims to evaluate and apply a fine-resolution global data set (Global Land Data Assimilation System with Noah Land Surface Model, GLDAS/Noah; 3-h, 0.25-degree) in a semiarid mesoscale basin (~15000 km^2). Four supporting objectives are proposed: (1) validating a Water and Energy Budget-based Distributed Hydrological Model (WEB-DHM) for GLDAS/Noah evaluation and application; (2) evaluating GLDAS forcing data (precipitation; near-surface air temperature, T_{air}; downward shortwave radiation, $R_{sw,d}$; downward longwave radiation, $R_{lw,d}$); (3) investigating GLDAS/Noah outputs (land surface temperature, LST; evapotranspiration; fluxes); (4) evaluating the applicability of GLDAS forcing in modeling basin-wide water cycles. Japanese 25-year reanalysis and in situ observations (precipitation; T_{air}; $R_{sw,d}$; discharge) are used for GLDAS/Noah evaluation. Main results include: (1) WEB-DHM can reproduce daily discharge, 8-day LST and monthly surface soil moisture (point scale) fairly well; (2) the GLDAS is of high quality for daily and monthly precipitation, T_{air}, monthly $R_{lw,d}$, while it overestimates monthly $R_{sw,d}$; (3) the GLDAS/Noah agrees well with the verified WEB-DHM and JRA-25 in terms of LST, upward shortwave and longwave radiation. While the net radiation, evapotranspiration, latent and sensible heat fluxes modeled by GLDAS/Noah are larger than WEB-DHM and JRA-25 simulations in wet seasons; (4) the basin-integrated discharges and evapotranspiration can be reproduced reasonably well by WEB-DHM fed with GLDAS forcing except linear corrections of $R_{sw,d}$. These findings would benefit the IWRM in ungauged or poorly gauged river basins around the world.

Citation: Wang, F., L. Wang, T. Koike, H. Zhou, K. Yang, A. Wang, and W. Li (2011), Evaluation and application of a fine-resolution global data set in a semiarid mesoscale river basin with a distributed biosphere hydrological model, *J. Geophys. Res.*, *116*, D21108, doi:10.1029/2011JD015990.

1. Introduction

[2] Accurate mesoscale modeling of the surface water and energy cycles is essential for proper understanding of hydrological and meteorological processes [e.g., *Chen and Dudhia*, 2001] and for water resources management. Land surface models (LSMs) are key tools for depicting interactions between the land surface and atmosphere [e.g., *Sellers et al.*, 1986, 1997; *Dirmeyer et al.*, 1999; *Bowling et al.*, 2003; *Rodell et al.*, 2005]. Over the past two decades, rapid progress has been made in the development of LSMs [*Sellers et al.*, 1986, 1996a; *Xue et al.*, 1991; *Koster and Suarez*, 1992b; *Liang et al.*, 1994; *Henderson-Sellers et al.*, 1995; *Chen et al.*, 1996; *Betts et al.*, 1997; *Koren et al.*, 1999; *Koster et al.*, 2000; *Chen and Dudhia*, 2001; *Dai et al.*, 2003; *Ek et al.*, 2003]. However, these LSMs are usually one-dimensional (1-D) vertical models [*Warrach et al.*, 2002; *Rigon et al.*, 2006] and generally not suitable for basin-scale water and energy studies, due to the absence or incomplete descriptions of slope hydrology and river routing. The slope hydrology affects the land–atmosphere exchanges of momentum, heat, and water through several nonlinear processes [*Tang et al.*, 2007]. A realistic representation of subgrid-scale variability would improve land surface modeling significantly [*Koster and Suarez*, 1992a; *Tang et al.*, 2007]. The strategy of coupling LSMs and distributed hydrology models (DHMs) potentially

[1]Institute of Water Resources and Flood Control, Faculty of Infrastructure Engineering, Dalian University of Technology, Dalian, China.
[2]Department of Civil Engineering, University of Tokyo, Tokyo, Japan.
[3]Institute of Tibetan Plateau Research, Chinese Academy of Sciences, Beijing, China.
[4]Nansen-Zhu International Research Center, Institute of Atmospheric Physics, Chinese Academy of Sciences, Beijing, China.
[5]Fengman Hydropower Plant, Jilin, China.

0148-0227/11/2011JD015990

improves the land surface representation and hydrological model prediction capabilities [*Pietroniro and Soulis*, 2003]. Inspired by this trend, several new DHMs appeared in recent years [e.g., *Tang et al.*, 2007; *Rigon et al.*, 2006; *Wigmosta et al.*, 1994].

[3] The new generation DHMs provide improved estimates of water and energy fluxes in basin scale with different size, but they usually need more meteorological forcing data than traditional water-balance DHMs. The forcing data include precipitation, radiation, near surface air temperature, humidity, pressure, and wind speed at subdaily resolution. The models will not produce realistic results if the forcing data are not accurate, no matter how sophisticated their depiction of land surface processes or how accurate their initial and boundary conditions are [*Cosgrove et al.*, 2003]. Errors in any of the forcing quantities (especially precipitation and solar radiation) can greatly impact simulations of soil moisture, runoff and latent and sensible heat fluxes [*Cosgrove et al.*, 2003; *Luo et al.*, 2003]. As such, a more robust approach is to make use of as much accuracy forcing data as possible [*Cosgrove et al.*, 2003]. Unfortunately, the multidecadal, high-resolution, realistic atmospheric forcing data are usually not readily available from observations in most cases [*Qian et al.*, 2006].

[4] The Global Land Data Assimilation System (GLDAS [*Rodell et al.*, 2004a]; based on the North American Land Data Assimilation System (NLDAS) project [*Mitchell et al.*, 2004; *Cosgrove et al.*, 2003]) ingests ground- and space-based observations, and executes simulations with multiple advanced LSMs driven by a land information system [*Kumar et al.*, 2006], aiming to optimally estimate terrestrial water and energy storages and fluxes. The observations are used in both model forcing (to avoid biases in atmospheric model-based forcing) and parameterization (to curb unrealistic model states) to constrain the modeled land surface states [*Rodell et al.*, 2004a]. The data used in driving GLDAS include precipitation (P), near-surface air temperature (T_{air}), downward shortwave ($R_{sw,d}$) and longwave ($R_{lw,d}$) radiation, specific humidity (Q_a), wind speed (U and V) and surface pressure (P_s) [*Rodell et al.*, 2004a]. The Noah LSM [*Chen et al.*, 1996; *Koren et al.*, 1999; *Betts et al.*, 1997; *Ek et al.*, 2003] driven by GLDAS (hereafter, GLDAS/Noah) provides high resolution outputs both temporally and spatially (3-h 0.25-degree). Since 2004, several evaluations and applications have been and are being implemented with GLDAS/Noah [*Koster et al.*, 2004; *Rodell et al.*, 2004b; *Kato et al.*, 2007; *Syed et al.*, 2008; *Yang and Koike*, 2008; *Zhang et al.*, 2008; *Yang et al.*, 2009b; *Zaitchik et al.*, 2010].

[5] The advanced GLDAS/Noah inspires us to investigate its applicability for basin scale water and energy budget study. Meanwhile, the high resolution inputs of GLDAS provide us the opportunity to force new generation DHMs in basin scale using the GLDAS forcing data and thus improve the integrated water resources management. The overarching objective of this paper is to evaluate the applicability of GLDAS/Noah (both inputs and outputs) for basin scale water and energy studies. To achieve this goal, the overarching objective is divided into 4 supporting objectives: (1) to validate a DHM in simulating water and energy budget for the evaluation and application of GLDAS/Noah (obj. 1); (2) to evaluate the accuracy of GLDAS forcing data (P, T_{air}, $R_{sw,d}$, and $R_{lw,d}$; obj. 2); (3) to investigate the performance of GLDAS/Noah outputs (LST, evapotranspiration, fluxes, etc.; obj. 3); and (4) to evaluate the applicability of GLDAS forcing data (P, T_{air}, $R_{sw,d}$, $R_{lw,d}$, etc.) in modeling (by DHMs) basin scale water cycles (obj. 4). In the study, opportunity also arises to examine WEB-DHM simulated monthly soil moisture compared with in situ observations (surface 10 cm). This paper is unique in that it tries to evaluate and apply a high-resolution global scale operational product (GLDAS/Noah) for basin scale water and energy studies. These results would provide reference for other regions where the observations are not available (or limited). The DHM used in this study is the Water and Energy Budget-based Distributed Hydrological Model (WEB-DHM [*Wang et al.*, 2009a, 2009b, 2009c]) and the study basin is a semi-arid mesoscale river basin locates in the Northeast part of China.

[6] This paper is organized as follows. Section 2 describes the methods. Section 3 provides results and discussions corresponding to the 4 objectives: section 3.1 evaluates WEB-DHM with in situ discharges and MODIS/Terra V5 land surface temperatures (LSTs); section 3.2 evaluates GLDAS forcing data (P, T_{air}, $R_{sw,d}$ and R_{lw}) against in situ observations (P, T_{air}, $R_{sw,d}$) and JRA-25 (P, T_{air}, $R_{sw,d}$ and R_{lw}). They are evaluated because the observations are available; section 3.3 investigates the performance of the GLDAS/Noah simulated LST, evapotranspiration (ET), upward shortwave ($R_{sw,u}$) and longwave radiation ($R_{lw,u}$), net radiation (R_n), latent heat flux (LE), sensible heat flux (H) and ground heat flux (G) through comparing with WEB-DHM simulations (LST, ET, $R_{sw,u}$, $R_{lw,u}$, R_n, LE, H, G) and JRA-25 product (ET, $R_{sw,u}$, $R_{lw,u}$, R_n, LE, H, G); section 3.4 verifies the applicability of GLDAS forcing data (P, $R_{sw,d}$, $R_{lw,d}$, T_{air}, Q_a, P_s, U and V) in basin-scale streamflow simulations. Conclusions and future directions are given in section 4.

2. Methods

2.1. Overview

[7] Four experiments (exp.1 – exp.4; Figure 1) are designed corresponding to 4 sub-objectives (obj.1 – obj.4). First (exp.1), a validation of the WEB-DHM (obj. 1) in simulating water and energy budgets is undertaken using ground-based discharge (*Q_obs*) at 2 major stream gauges (Yangzishao and Wudaogou, Figure 2b) and MODIS/Terra V5 8-day LSTs [*Wan*, 2008] (described in section 2.5) observations from 2000 to 2006 (Figure 1). River discharges spatially integrate all upstream hydrological processes and are recorded with good accuracy [*Zaitchik et al.*, 2010]. Therefore, they can be used to evaluate the WEB-DHM water budget. The LST is a key parameter in the surface energy budget [*Bertoldi et al.*, 2010] since it is the result of all surface–atmosphere interactions and energy fluxes between the atmosphere and ground. Furthermore, the LST is available through remote sensing on a global scale with high resolution and can be used to validate the energy budget described by the WEB-DHM.

[8] Second (exp.2), an intercomparison (Figure 1) of atmospheric forcing data is executed between GLDAS (P, T_{air}, $R_{sw,d}$ and $R_{lw,d}$), ground-based observations (P, T_{air} and $R_{sw,d}$), JRA-25 (described in 2.6.2) operational product (P, T_{air}, $R_{sw,d}$ and $R_{lw,d}$) and WEB-DHM inputs ($R_{sw,d}$ and

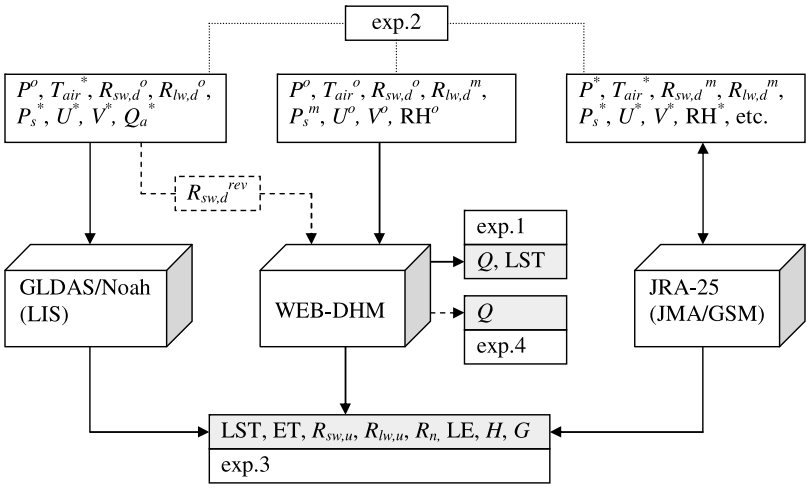

Figure 1. The flowchart of this study. The superscript '*o*', '*', and '*m*' mean observation (or observation-based), assimilation, and model simulation, respectively (see sections 2.4 and 2.6); the shaded box means model output variables; the dashed line means WEB-DHM fed with GLDAS (and revised) forcing data. The exp.1 – exp.4 means four experiments, corresponding to obj.1 – obj.4. P: precipitation; T_{air}: near-surface air temperature; $R_{sw,d}$, $R_{lw,d}$: downward shortwave and longwave radiation; Q_a: specific humidity; RH: relative humidity; U, V: wind speed; P_s: surface pressure; Q: river discharge; LST: land surface temperature; ET: evapotranspiration; $R_{sw,u}$, $R_{lw,u}$: upward shortwave and longwave radiation; R_n: net radiation; LE, H, G: latent, sensible and ground heat fluxes. The LST (exp.3) is only available for GLDAS/Noah and WEB-DHM.

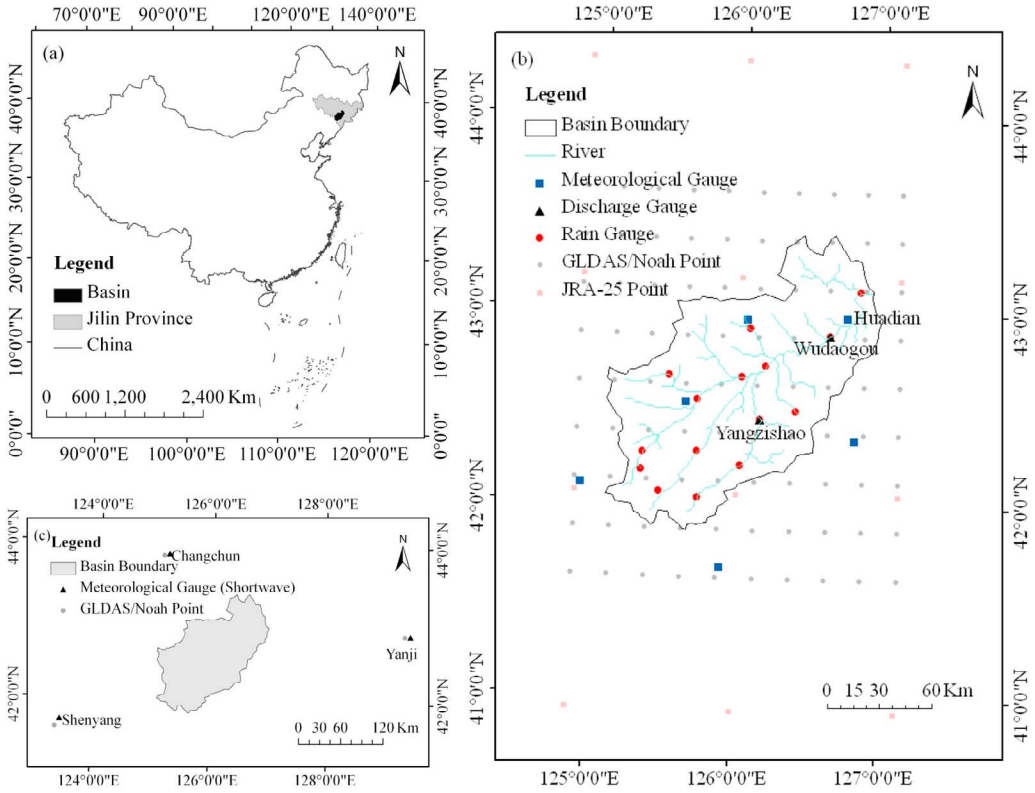

Figure 2. The upper reach of the Second Songhua River basin: (a) the location within China and (b and c) the data sets used in this study. The meteorological gauges in Figure 2c measure downward shortwave radiation, while the meteorological gauges in Figure 2b measure relative humidity, wind speed, sunshine duration, daily maximum and minimum temperature, etc.

Table 1. Table of WEB-DHM Simulation Performed[a]

Experiment	Purpose	Input	Output	Period
Exp. 1	obj. 1	Observed (or observation-based) P, T_{air}, $R_{sw,d}$, $R_{lw,d}$, U, V, RH, P_s	LST, *Q_WEB-DHM*	2000–2006
Exp. 3	obj. 3	Observed (or observation-based) P, T_{air}, $R_{sw,d}$, $R_{lw,d}$, U, V, RH, P_s	LST, ET, $R_{sw,u}$, $R_{lw,u}$, R_n, LE, H, G	2000–2006
Exp. 4	obj. 4	GLDAS forcing data[b]	*Q_GLDAS*	2000–2006
Exp. 4	obj. 4	Revised GLDAS forcing data[b]	*Q_GLDAS_rev*	2000–2006

[a]See section 2.1.
[b]GLDAS forcing include P, T_{air}, $R_{sw,d}$, $R_{lw,d}$, Q_a, P_s, U and V. It should be noted that the exp. 2 does not include any WEB-DHM simulation. All the experiments are executed in the same basin (USSR).

$R_{lw,d}$) to evaluate the accuracy of the GLDAS forcing data (obj. 2).

[9] Third (exp.3), the outputs of GLDAS/Noah (LST, ET, $R_{sw,u}$ $R_{lw,u}$, R_n, LE, H and G) are compared with WEB-DHM simulations (LST, ET, $R_{sw,u}$, $R_{lw,u}$, R_n, LE, H, and G) and JRA-25 operational product (ET, $R_{sw,u}$, $R_{lw,u}$, R_n, LE, H, and G) (Figure 1) to investigate the performance of GLDAS/Noah in reproducing water and energy cycles (obj. 3).

[10] Fourth (exp.4), experiments are designed to test the performance of GLDAS forcing data (P, $R_{sw,d}$, $R_{lw,d}$, T_{air}, Q_a, P_s, U and V) in simulating discharge (obj.4) by using WEB-DHM (Figure 1). The experimental period is from 24 February 2000 to 31 December 2006. Two experiments are executed. (1) WEB-DHM is driven by using all of the original GLDAS forcing data. (2) According to evaluation results of exp.2, the original GLDAS forcing is corrected based on observation. The GLDAS forcing data correction includes two steps. First, the scatterplots of daily forcing data (e.g., $R_{sw,d}$) between in situ observations and GLDAS from March 2000 to December 2006 are drawn. Second, the linear regression equations derived from the scatterplots are used as correction functions. And then the WEB-DHM is driven by using the corrected forcing and the other forcing data remains the same. The output discharges (*Q_GLDAS* and *Q_GLDAS_rev*) at Wudaogou station are examined by using measured streamflows (*Q_obs*) (Figure 2b).

[11] In this study, GLDAS/Noah and JRA-25 data are obtained from their operational products, while the WEB-DHM outputs are obtained by running the model 3 times driven by different forcing data (see Table 1). (1) WEB-DHM is forced by observed (or observation-based) data (P, $R_{sw,d}$, $R_{lw,d}$, T_{air}, relative humidity-RH, P_s, U and V). The simulated discharge (*Q_WEB-DHM*) and LST are evaluated through *Q_obs* and MODIS LST (described in 2.5). The simulated LST, ET, $R_{sw,u}$ $R_{lw,u}$, R_n, LE, H and G are then compared with corresponding GLDAS/Noah simulations; (2) WEB-DHM is driven by original GLDAS forcing data (P, $R_{sw,d}$, $R_{lw,d}$, T_{air}, Q_a, P_s, U and V); (3) WEB-DHM is driven by corrected GLDAS forcing data. The simulated discharges from (2) and (3) (*Q_GLDAS* and *Q_GLDAS_rev*) are evaluated by comparing with *Q_obs*.

[12] All experiments are carried out in the same semi-arid river basin. The period from March 2000 to December 2006 was chosen for this study, as data exist in this period. Furthermore, this near 7-year period includes both arid and semiarid periods, which are helpful in understanding the water and energy cycles under different climatic conditions. Sections 2.2 to 2.7 describe the study basin, the WEB-DHM model, in situ observations, satellite observations, the operational products (GLDAS/Noah and JRA-25) and evaluation criteria.

2.2. Study Region

[13] The upper Second Songhua River Basin (USSR) covers longitudes from 124.98°E to 127.06°E and latitudes from 41.83°N to 43.44°N (Figure 2a), and has a catchment area of about 14,700 km^2. The average annual precipitation is approximately 700 mm. The mean annual temperature ranges from 1.4°C to 4.3°C, and the average maximum is 23°C to 24°C in July and the average minimum is −17°C in January. This region has been chosen because it is representative of a semiarid environment and comprehensive data are available for this study. This basin is characterized by temperate semiarid continental climate. The annual precipitation is uneven with 60–90% precipitation concentrated in flood season (from June to September) [*Asian Development Bank*, 2002]. This area is threatened by spring drought and summer flood.

2.3. The WEB-DHM Model

[14] The distributed biosphere hydrological model, WEB-DHM [*Wang et al.*, 2009a, 2009b, 2009c], was developed by fully coupling a simple biosphere scheme (SiB2) [*Sellers et al.*, 1996a] with a geomorphology-based hydrological model (GBHM) [*Yang et al.*, 2002, 2004a; *Wang et al.*, 2010a] toward the goal of consistent descriptions of water, energy and CO_2 fluxes in a basin scale. Several evaluations, improvements and applications have been executed with WEB-DHM [*Wang et al.*, 2010b; *Shrestha et al.*, 2010; *Saavedra Valeriano et al.*, 2010; *Jaranilla-Sanchez et al.*, 2011]. The WEB-DHM background in this study is the same as in the study by *Wang et al.* [2009b]. This paper only briefly summarizes the model's structure and LST calculation method, because the LST is used in this study to analyze results. A complete description was given by *Wang et al.* [2009a, 2009b, 2009c].

[15] Figure 3 illustrates the general model structure. First, the land surface sub-model (the hydrologically improved SiB2 [*Wang et al.*, 2009c]) is used to describe the turbulent fluxes (energy, water and CO_2) between the atmosphere and land surface for each model cell. Second, the hydrological sub-model simulates both surface and subsurface runoff with cell-hillslope discretization, and then calculates flow routing in the river network.

[16] In this study, the WEB-DHM LST was estimated following *Wang et al.* [2009b].

$$T_{\mathrm{sim}} = \left[V \times T_c^4 + (1 - V) \times T_g^4\right]^{1/4}, \tag{1}$$

$$V = \mathrm{LAI}/\mathrm{LAI}_{\max}, \tag{2}$$

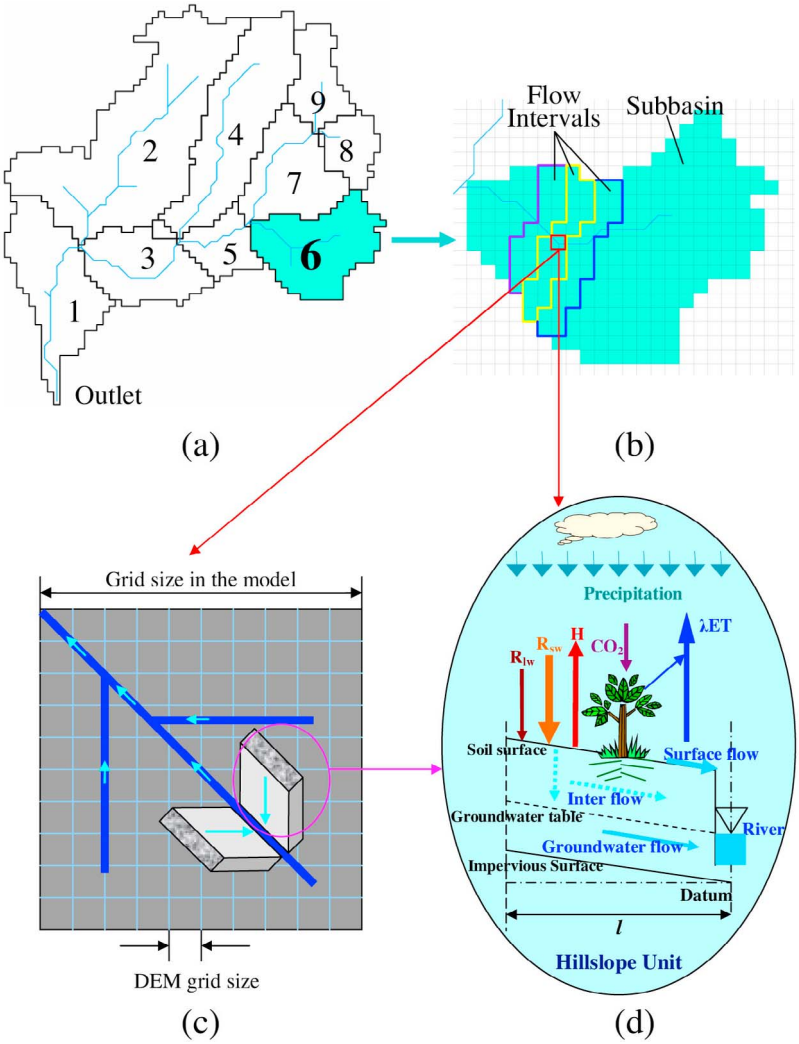

Figure 3. Overall structure of WEB-DHM model: (a) division from a basin to sub-basins; (b) subdivision from a sub-basin to flow intervals comprising several model grids; (c) discretization from a model grid to a number of geometrically symmetrical hillslopes and (d) process descriptions of the water moisture transfer from atmosphere to river. Here, SiB2 is used to describe the transfer of the turbulent fluxes (energy, water, and CO_2 fluxes) between atmosphere and land surface for each model grid, where R_{sw} and R_{lw} are downward shortwave radiation and longwave radiation, respectively; H is the sensible heat flux; and λ is the latent heat of vaporization. GBHM simulates both surface and subsurface runoff using grid-hillslope discretization, and then simulates flow routing in the river network.

where T_{sim} is the simulated LST; V is green vegetation coverage; T_c is the temperature of the canopy; T_g is the temperature of the soil surface; LAI is the leaf area index; and LAI_{max} is the maximum LAI value defined following *Sellers et al.* [1996b]. LAI is derived from MOD11A2 V5 1-km 8-day product (see section 2.5) and it is time-varying on both seasonal and inter-annual scales.

2.4. In Situ Observations

[17] The ground-based meteorological observations include daily precipitation, relative humidity, wind speed, daily maximum temperature, daily minimum temperature, daily average temperature and sunshine duration. They were obtained from China Meteorological Administration (CMA). There are 15 rain gauges in the basin (Figure 2b) and hourly precipitation data were downscaled from daily rain gauge observation data using a stochastic method [*Yang et al.*, 2004b]. Data from 6 meteorological sites (Figure 2b) in the basin were taken. Hourly temperatures were calculated from daily maximum and minimum temperatures using the TEMP model [*Parton and Logan*, 1981]. The estimated temperatures were further evaluated using the daily average temperature. Downward solar radiation was estimated from sunshine duration, temperature, and humidity using a hybrid model developed by *Yang et al.* [2001, 2006]. Longwave radiation and the cloud fraction were obtained from JRA-25 data [*Onogi et al.*, 2007] (http://jra.kishou.go.jp/). Air pressure was estimated according to the altitude [*Yang et al.*, 2006]. These meteorological data were then interpolated to 1000 m model cells through

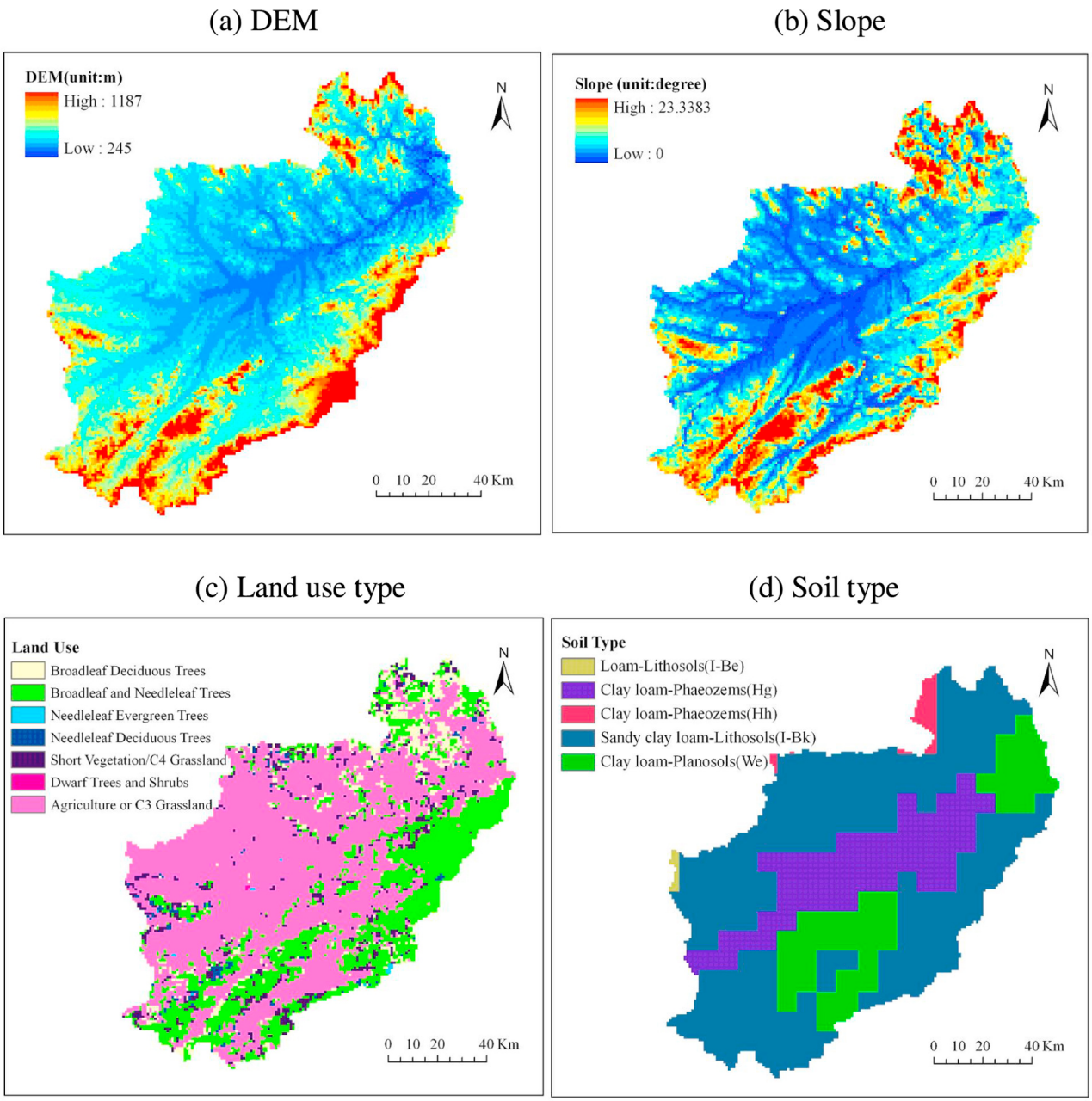

Figure 4. DEM, grid slope, land use and soil type used by WEB-DHM.

inverse-distance weighting. The surface air temperature inputs were further modified with a lapse rate of 6.5 K/km considering the elevation differences between the model cells and meteorological stations.

[18] The ground-based daily streamflow is used to calibrate and evaluate the WEB-DHM model. There are 2 major discharge gauges located in the basin (Figure 2b); observations are available for Yangzishao from 2000 to 2006 and for Wudaogou from 2000 to 2005.

[19] The surface soil moistures observed at Huadian station (Figure 2b) are used here to evaluate WEB-DHM simulations. The soil moisture was measured at surface 10 cm by the gravimetric technique in the warm season [*Wang and Zeng*, 2011]. The monthly values are available from 2000 to 2006.

[20] The downward shortwave radiations observed at Changchun, Shenyang and Yanji stations (Figure 2c) obtained from China Meteorological Administration (CMA) are used to evaluate the GLDAS/Noah product. The three stations are located around the study basin and the daily data are available from 2000 to 2006.

2.5. Satellite Observations

[21] DEM data were obtained from the United States Geological Survey (USGS) Seamless Data Distribution System (http://seamless.usgs.gov/) and the subgrid topography was described by a 100 m DEM. The elevation of the basin varies from 245 to 1187 m (Figure 4a) and the grid slopes vary from 0 to 23 degrees (Figure 4b). Land-use data were obtained from the USGS (http://edc2.usgs.gov/glcc/

glcc.php). The land-use types have been reclassified to SiB2 land-use types for the study [*Sellers et al.*, 1996a]. There are 7 land-use types, with agriculture or C3 grassland being the main type (Figure 4c). Soil data were obtained from the *Food and Agriculture Organization* (*FAO*) [2003] global data product. There are 5 kinds of soil in the basin, with sandy clay loam being the dominant type (Figure 4d).

[22] Static vegetation parameters including morphological, optical and physiological properties defined by *Sellers et al.* [1996b] were used in this study. Dynamic vegetation parameters including the leaf area index (LAI) and the fraction of photosynthetically active radiation (FPAR) absorbed by the green vegetation canopy were obtained from the MOD15A2 1-km 8-day products [*Myneni et al.*, 1997]. They were downloaded through the Warehouse Inventory Search Tool (WIST, https://wist.echo.nasa.gov/~wist/api/imswelcome/). Data from 18 February 2000 are available.

[23] LSTs obtained from the Moderate Resolution Imaging Spectroradiometer (MODIS) aboard the Terra (EOS AM) satellite are used to validate the WEB-DHM performance in representing the basin-scale energy budget. The MOD11A2 V5 1-km 8-day product [*Wan*, 2008], which is available from 5 March 2000, is used in this study. The MODIS LSTs were observed during the day around 10:30 and at night around 22:30 (both local time). These data were downloaded through WIST.

2.6. The Operational Products

2.6.1. GLDAS/Noah

[24] GLDAS [*Rodell et al.*, 2004a] integrates satellite- and ground-based observations for parameterizing, forcing and constraining a suite of offline (uncoupled) land surface models. GLDAS aims to generate optimal fields of land surface states and fluxes. Currently, GLDAS drives 4 LSMs: Mosaic [*Koster and Suarez*, 1992b], Noah [*Chen et al.*, 1996; *Koren et al.*, 1999; *Ek et al.*, 2003; *Betts et al.*, 1997], the Community Land Model (CLM) [*Dai et al.*, 2003] and the Variable Infiltration Capacity (VIC) model [*Liang et al.*, 1994]. In this study, we use the GLDAS/Noah Land Surface Model L4 3-h 0.25-degree × 0.25-degree subsetted (GLDAS_NOAH025SUBP_3H) product (downloaded from http://disc.sci.gsfc.nasa.gov/hydrology/data-holdings) since the high resolution data are more desirable for the basin-scale study (14700 km^2). The 3-h GLDAS/Noah data are available from 24 February 2000. The GLDAS data were described in more detail by *Rodell et al.* [2004a] and *Kato et al.* [2007]. A total of 90 GLDAS/Noah cells are used for the study basin (see Figure 2b).

[25] GLDAS precipitation is based on the NOAA Climate Prediction Center's operational global 2.5 degree 5-day Merged Analysis of Precipitation (CMAP) [*Xie and Arkin*, 1997; *Xie et al.*, 2003] which blends both satellite (IR and microwave) and gauge observations [*Kato et al.*, 2007]. By using NOAA's Global Data Assimilation System (GDAS) [*Derber et al.*, 1991] precipitation analyses, GLDAS precipitation is spatially and temporally downscaled [*Rodell et al.*, 2004a; *Kato et al.*, 2007]. GLDAS near-surface air temperature is obtained from NOAA's GDAS operational analyses [*Rodell et al.*, 2004a; *Kato et al.*, 2007], and then it is adjusted adiabatically to the GLDAS elevation definition based on *Cosgrove et al.* [2003]. GLDAS $R_{sw,d}$ and $R_{lw,d}$ are derived from cloud and snow products of the U.S. Air Force Weather Agency's (AFWA) Agricultural Meteorological modeling system (AGRMET) [*Rodell et al.*, 2004a; *Kato et al.*, 2007] by using AFWA-supplied algorithms of *Shapiro* [1972] and *Idso* [1981], respectively.

2.6.2. JRA-25

[26] Japan Meteorological Agency (JMA) and Central Research Institute of Electric Power Industry (CRIEPI) jointly produced a Japanese 25-year reanalysis product (JRA-25 [*Onogi et al.*, 2007]; http://jra.kishou.go.jp/) employing the JMA numerical assimilation and forecast system, with the goal of achieving high-quality analysis in the Asian region. The JRA-25 forecast system employs a low-resolution version of the operational JMA Global Spectral Model (GSM), which has a spectral resolution of T106 (around 120 km horizontal grid size) and 40 vertical layers (L40) up to 0.4 hPa [*Onogi et al.*, 2007; *Japan Meteorological Agency* (*JMA*), 2007, chapters 3.5, 3.11, and 4.2]. The assimilation system used in JRA-25 is a 3-dimentional variational (3D-Var) analysis method with 6-h global data assimilation cycles [*Onogi et al.*, 2007; *JMA*, 2007, chapters 3.5, 3.11, and 4.2]. JRA-25 data have been recorded every 6 h since 1979. Twelve JRA-25 cells were used in this study (Figure 2b).

[27] The JRA-25 variables are obtained from both model simulations and data assimilation techniques. The $R_{sw,d}$ is calculated by a two-stream formulation based on delta-Eddington approximation [*Joseph et al.*, 1976; *Coakley et al.*, 1983; *Briegleb*, 1992]. The $R_{lw,d}$ is modeled by a wide-band flux emissivity method for four spectral bands [*Onogi et al.*, 2007]. The JRA-25 assimilated variables include temperature, wind speed, relative humidity, surface pressure at model surface, radiative brightness temperature and precipitable water [*Onogi et al.*, 2007]. The JRA-25 T_{air} is assimilated from radiosonde observations [*Onogi et al.*, 2007]. The JRA-25 precipitation is assimilated from microwave radiometer sensor Special Sensor of Microwave Imager (SSM/I) on board the Defense Meteorological Satellite Program (DMSP) satellite [*Onogi et al.*, 2007]. The radiative brightness temperature (T_b) is assimilated from TIROS Operational Vertical Sounder (TOVS). More detailed descriptions were provided by *Onogi et al.* [2007].

2.7. Evaluation Criteria

[28] Several statistical variables are used to evaluate the performances of the WEB-DHM, the GLDAS/Noah and the JRA-25:

$$\mathrm{NS} = 1 - \sum_{i=1}^{n}(X_{oi} - X_{si})^2 / \sum_{i=1}^{n}(X_{oi} - \overline{X}_0)^2, \tag{3}$$

$$\mathrm{RB} = \left(\sum_{i=1}^{n} X_{si} - \sum_{i=1}^{n} X_{oi}\right) / \left(\sum_{i=1}^{n} X_{oi}\right) \times 100\%, \tag{4}$$

$$\mathrm{MBE} = \left(\sum_{i=1}^{n} X_{si} - \sum_{i=1}^{n} X_{oi}\right) / n \times 100\%, \tag{5}$$

$$\mathrm{RMSE} = \left[\frac{1}{n} \times \sum_{i=1}^{n}(X_{si} - X_{oi})^2\right]^{\frac{1}{2}}, \tag{6}$$

Table 2. Basin-Averaged Values of the Parameters Used in the Study

Symbol	Parameters	Basin-Averaged Value	Source
θs	Saturated soil moisture content	0.48	*FAO* [2003]
θr	Residual soil moisture content	0.08	*FAO* [2003]
α	Van Genuchen's parameter	0.02	Optimization
n	Van Genuchen's parameter	1.60	Optimization
Dr(m)	Root depth (D1 + D2)	1.17	*Sellers et al.* [1996b]
Ks(mm/h)	Saturated hydraulic conductivity for soil surface	37.81	Optimization
anik	Hydraulic conductivity anisotropy ratio	53.83	Optimization
Sstmax(mm)	Maximum surface water storage	8.00	Optimization

where X_{oi} is the observed (ground-based or satellite-) value; X_{si} is the simulated (WEB-DHM, JRA-25 or GLDAS/Noah) value; n is the total number of time series for comparison; and $\overline{X}_0$ is the mean value of X_{oi} over the comparison period. NS refers to Nash Sutcliffe [*Nash and Sutcliffe*, 1970]. The higher NS is, the better the model performs. A perfect fit should have a NS value equal to one. RB refers to relative bias. The lower RB, MBE or RMSE is, the better the model performs. A perfect fit should have RB, MBE or RMSE equal to zero. Since the observations are imperfect as well, the RB, MBE and RMSE should never be zero.

3. Results and Discussion

3.1. Evaluation of the WEB-DHM for the Study Region

[29] The WEB-DHM has been carefully calibrated with daily discharges at Yangzishao station (Figure 2b) for 2001 before its evaluation. The calibration has 2 steps. First, the initial conditions were obtained by running the model several times with forcing data of year 2000 until a hydrological equilibrium was reached. Second, a trial and error method is used to optimize several parameters by matching the simulated and observed daily streamflow at Yangzishao station (Figure 2b) using the data of year 2001. Both NS and RB (defined in equations (3) and (4)) are used to evaluate the model performance. The calibrated parameters include saturated hydraulic conductivity for soil surface (*Ks*), hydraulic conductivity anisotropy ratio (*anik*), maximum surface water storage (*Sstmax*), and Van Genuchen's parameter (α and n). The basin-averaged parameters used in this model are described in Table 2. An evaluation of the WEB-DHM in simulating water and energy budgets is then undertaken using ground-based discharge at 2 major stream gauges (Yangzishao and Wudaogou, Figure 2b) and MODIS/Terra V5 8-day LSTs [*Wan*, 2008] observations from 2000 to 2006.

3.1.1. Water Budget

[30] Figure 5 shows the daily discharge (Q) at Yangzishao and Wudaogou simulated by the WEB-DHM compared with measured value (Figure 2b). Figure 5a reveals that both the peak and base flows at Yangzishao are well reproduced from 2000 to 2006 with NS equal to 0.717 and RB equal to −6.37%. The simulated Q at Wudaogou (Figure 5b) from 2000 to 2005 also agrees well with the observations with NS equal to 0.810 and RB equal to 5.60%.

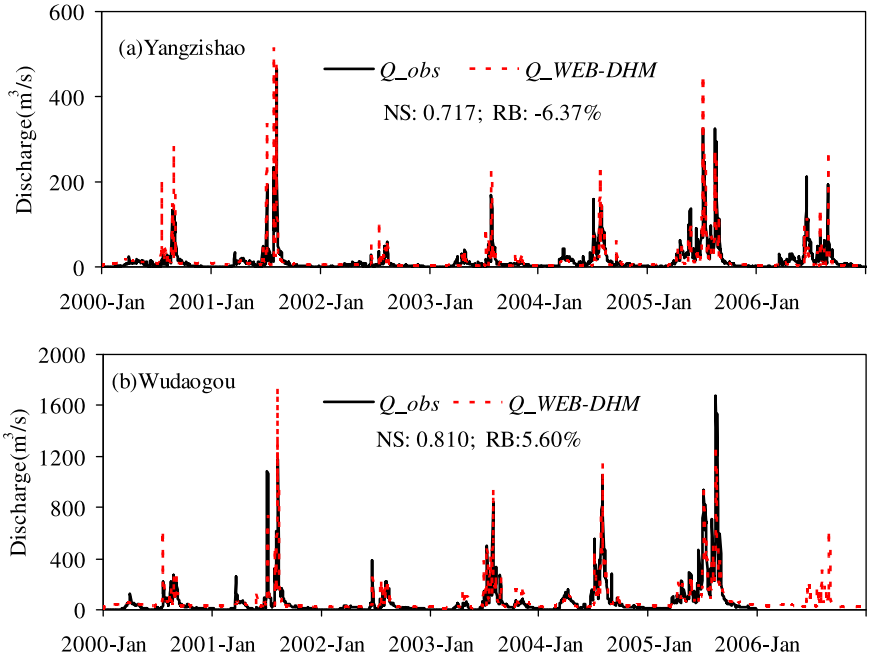

Figure 5. Observed and WEB-DHM simulated streamflows at (a) Yangzishao and (b) Wudaogou station from 2000 to 2006.

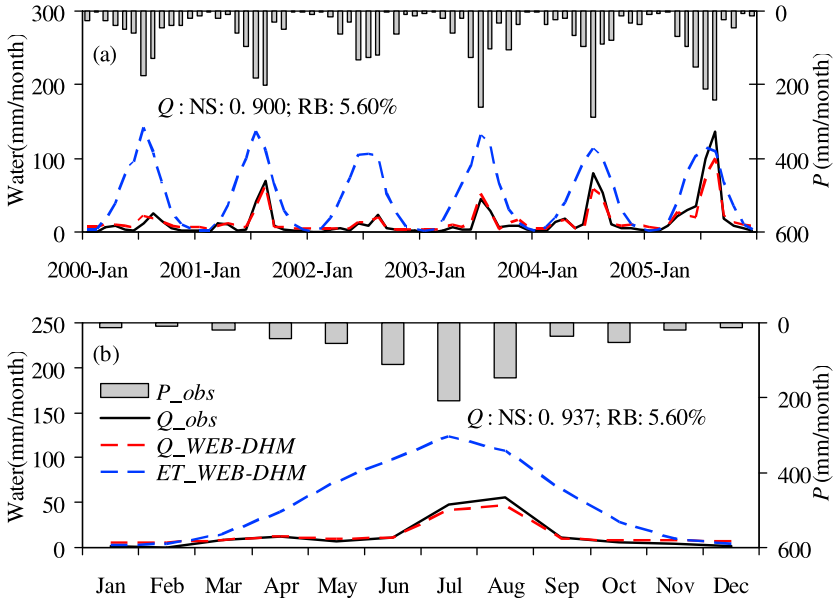

Figure 6. (a) Time series and (b) 6-year inter-annual mean monthly precipitation (*P*), WEB-DHM simulated evapotranspiration (*ET_WEB-DHM*), observed discharge (*Q_obs*) and WEB-DHM simulated discharge (*Q_WEB-DHM*) for the Wudaogou subbasin from 2000 to 2005.

[31] Figure 6 plots the monthly and 6-years (2000–2005) mean monthly variations in *Q* simulated by the WEB-DHM and compares them with observations. Time series of monthly observed precipitation (*P*), simulated evapotranspiration (ET), and observed and simulated *Q* for the upstream of the Wudaogou gauge are shown in Figure 6a. The *Q* of WEB-DHM simulations agree fairly well with observations with RB and NS equal to 5.60% and 0.900, respectively. Figure 6b shows the 6-years (2000–2005) mean monthly time series of water balance components, showing overall good agreement of *Q* between WEB-DHM outputs and observations with RB and NS equal to 5.60% and 0.937, respectively.

3.1.2. Energy Budget

[32] Figure 7 shows the 8-day LSTs of the WEB-DHM simulation (LST_WEB-DHM) and MODIS/Terra product (LST_MODIS) from March 2000 to December 2006 in the time series. The valid time of MODIS LSTs for this region is around 10:30 and 22:30 at local time. The simulation results show that LSTs are well reproduced except that LST_WEB-DHM is slightly greater than LST_MODIS with MBE equal to 2.17 K during the day (Figure 7a) and MBE equal to 2.50 K at night (Figure 7b). The scatterplots of LSTs are also given for both day and night (Figures 7c and 7d), with the correlation coefficient (*R*) equal to 0.9856 and 0.9896 for day and night, respectively. These results confirm the general good performance of the WEB-DHM in simulating basin-averaged LSTs.

[33] Figure 8 shows the seasonal spatial distribution differences of the daytime LSTs between model simulations and MODIS/Terra observations (WEB-DHM minus MODIS). In general, the spatial variations in LSTs are well simulated by the WEB-DHM. The basin average values of LSTs are 287.49 K, 298.40 K, 285.31 K and 261.46 K for MODIS/Terra, while they are 290.16 K, 302.84 K, 288.09 K and 259.83 K for WEB-DHM. The LSTs of WEB-DHM are overestimated in spring (2.66 K), summer (4.44 K) and autumn (2.78 K) while they are underestimated in winter (−1.62 K). The uncertainty may be attributed to the homogeneous lapse rate of temperature (γ = 6.5 K/km) used in this study for modifying T_{air}, since γ is variable with season, altitude and region. The uncertainty in linear calculation of green vegetation coverage (*V*, see equation (2)) also affects the simulation of soil surface temperature (T_g) and LST.

3.1.3. Summary

[34] The objective of section 3.1 was to validate the WEB-DHM in simulating spatially integrated streamflows and the basin-wide LSTs. In summary, the WEB-DHM has demonstrated good accuracy in representing the water and energy cycles in the upper Second Songhua River basin. This is the first study that WEB-DHM is evaluated with comprehensive observations in a semi-arid environment. Results show that the outputs from the calibrated WEB-DHM are reliable and thereby can be used to evaluate other operational products (e.g., GLDAS/Noah).

3.2. Comparing GLDAS Forcing Data With in Situ Observations, JRA-25, and WEB-DHM

3.2.1. Daily Scale

[35] Daily precipitation (*P*) and the near-surface air temperature (T_{air}) obtained from GLDAS and JRA-25 are compared with ground-based observations in Figure 9.

[36] Figures 9a and 9b plot the basin-averaged daily *P* used in GLDAS and JRA-25 against ground-based observation. The *R*, MBE and RMSE between GLDAS results and observations are 0.7599, 0.06 mm/day and 3.48 mm/day, respectively, while they are 0.5851, 0.58 mm/day and 6.39 mm/day between JRA-25 results and observations. All the statistics show that GLDAS is more consistent than JRA-25 with the observations. The rough spatial resolution of JRA-25 data (about 1.125 degrees) may miss localized precipitation events. Many studies [e.g., *Gottschalck et al.*,

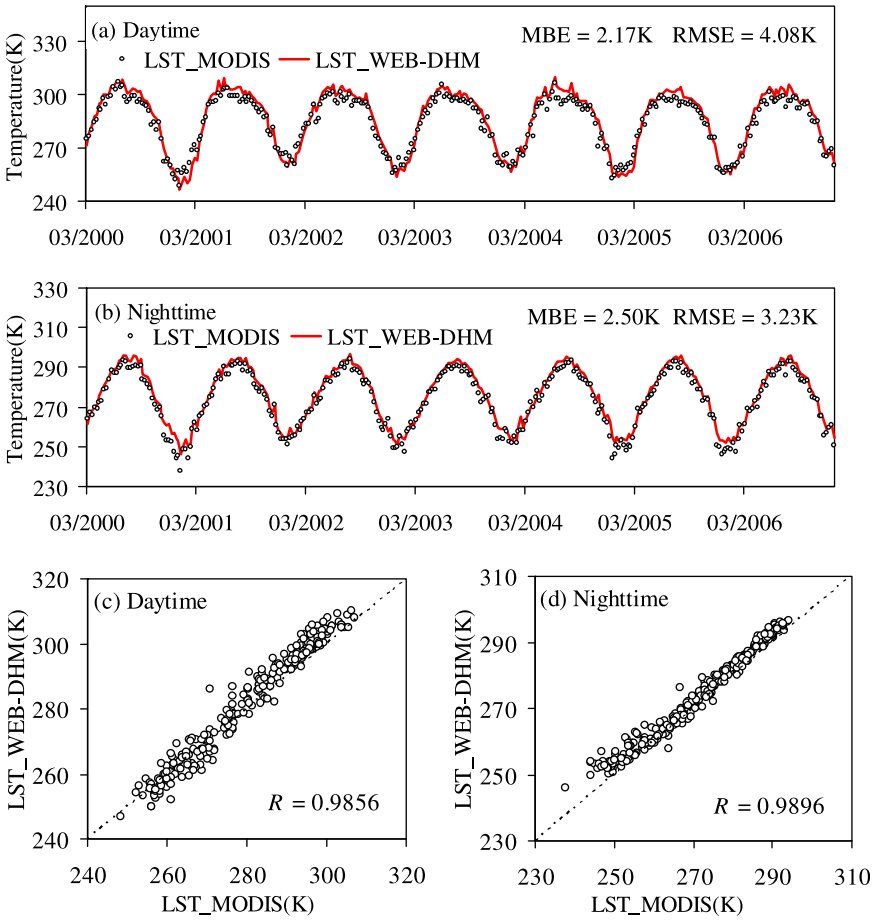

Figure 7. Comparison of 8-daily LSTs between WEB-DHM simulations (T_{sim}) and MODIS observations (T_{obs}) during (a, c) daytime and (b, d) nighttime averaged for the basin from March 2000 to December 2006. Time series (Figures 7a and 7b) and scatterplots (Figures 7c and 7d).

2005; *Zaitchik et al.*, 2010] have shown that the precipitation used in GLDAS has low bias relative to a number of earlier precipitation data sets that were used during development of LSMs. The results obtained in this study confirm the relatively good accuracy of GLDAS precipitation.

[37] Figures 9c and 9d plot the daily T_{air} used in GLDAS and JRA-25 and compare them with the ground-based observations. T_{air} is well represented by GLDAS and JRA-25 with R exceeding 0.9900 in both cases. The MBE and RMSE for GLDAS are −0.40 K and 1.70 K, respectively, while for JRA-25, the MBE and RMSE are 1.07 K and 2.09 K, respectively.

3.2.2. Monthly Scale

[38] Figures 10a and 10b compare monthly precipitation (P) and near-surface air temperature (T_{air}) between GLDAS, JRA-25 and ground-based observations in time series. Figures 10c and 10d compare monthly downward shortwave ($R_{sw,d}$) and longwave radiation ($R_{lw,d}$) between GLDAS, JRA-25 and WEB-DHM in time series. Figures 11a–11h are the corresponding scatterplots of Figures 10a–10d.

[39] Figure 10a reveals that GLDAS precipitation agrees fairly well with the observed precipitation, while JRA-25 precipitation has a large positive bias. The corresponding scatterplots (Figures 11a and 11b) show that the MBE is 1.86 mm/month between GLDAS and the observations, and this is much lower than that between JRA-25 and the observations. It has been reported [*Yang et al.*, 2009b; *Yang and Koike*, 2008] that the accumulated precipitation amount of JRA-25 is greater than that observed while GLDAS performed better than JRA-25 in a study of the Central Tibetan Plateau and a Mongolian semiarid region. This result further demonstrates the accuracy of precipitation used in GLDAS. This can be explained by the different precipitation products used in GLDAS and JRA-25. The GLDAS precipitation is based on the CMAP product [*Xie and Arkin*, 1997; *Xie et al.*, 2003] which merged rain gauge observations and five sets of satellite estimates derived from the infrared (IR), outgoing longwave radiation (OLR), Microwave Sounding Unit (MSU), microwave (MW) scattering, and emission from SSM/I, while the JRA-25 precipitation is assimilated from satellite (SSM/I). As previous studies mentioned [*Xie and Arkin*, 1997; *Xie et al.*, 2003; *Gottschalck et al.*, 2005], the rain gauge and satellite merged precipitation tends to produce relatively better analysis of global precipitation than satellite-only estimates because it takes advantage of the strength of each individual source.

[40] Figure 10b shows the T_{air} of GLDAS, JRA-25 and ground-based observations. There are no obvious differences except that JRA-25 gives slightly higher values than

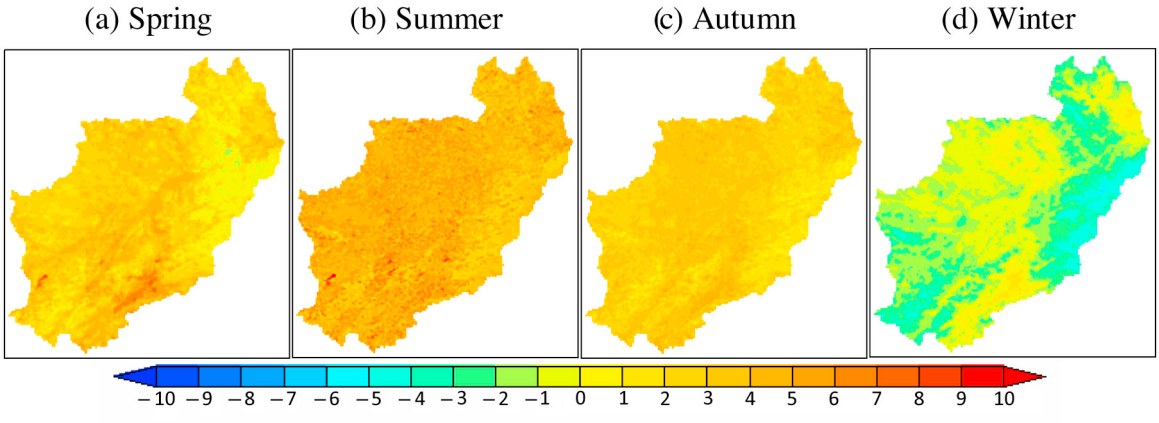

Figure 8. The differences of daytime LSTs (unit: K) between WEB-DHM and MODIS/Terra in (a) Spring (MAM), (b) Summer (JJA), (c) Autumn (SON), and (d) Winter (DJF) from March 2000 to December 2006.

GLDAS and the observations in winter. The small MBE seen in Figures 11c and 11d (−0.40 K and 1.07 K) and the small RMSE (0.95 K and 1.68 K) also indicate good consistency in T_{air} between simulations and observations.

[41] Figure 10c shows the level of downward shortwave radiation ($R_{sw,d}$) for GLDAS, the WEB-DHM and JRA-25. It is clear that $R_{sw,d}$ for GLDAS is obviously higher than that of the WEB-DHM and JRA-25 in summer. Figures 11e and 11f show that MBE between the WEB-DHM and GLDAS is −10.83 W/m^2 and that between JRA-25 and GLDAS is −11.01 W/m^2.

[42] The $R_{sw,d}$ of GLDAS is further investigated by using ground-based observations. Table 3 compares $R_{sw,d}$ at Changchun, Shenyang, Yanji stations (Figure 2c) and study basin. GLDAS overestimates $R_{sw,d}$ significantly during warm season (from April to August) with MBE larger than 52.66 W/m^2 and during cold season (from September to March) with MBE larger than 15.14 W/m^2 for all the three stations (Table 3). Averaged at the whole basin, GLDAS overestimates $R_{sw,d}$ with MBE equal to 54.61 W/m^2 and 16.95 W/m^2 in warm and cold seasons, respectively (Table 3).

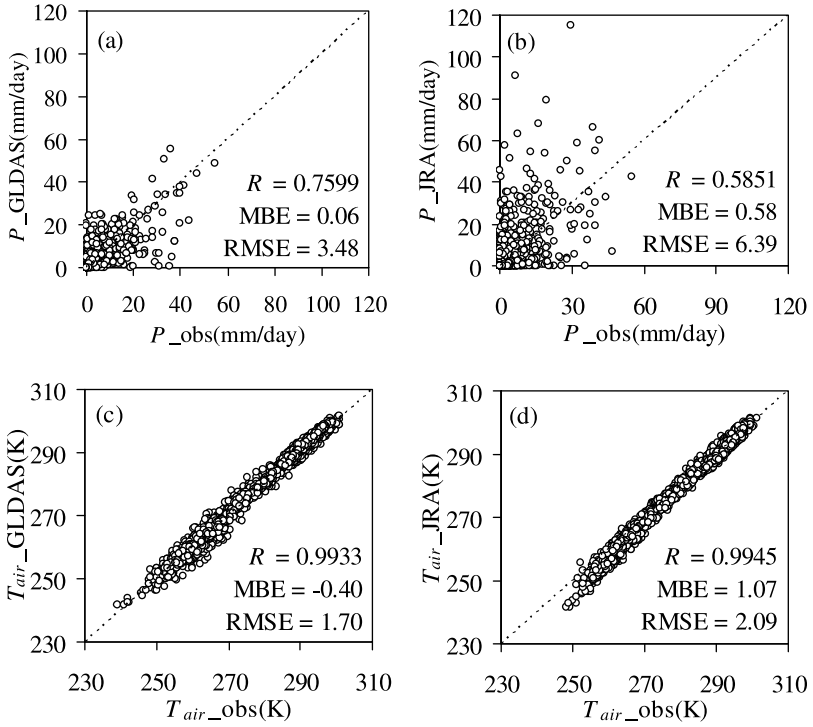

Figure 9. Scatterplots of daily values averaged at the whole basin between ground-based observations and GLDAS and JRA-25 products from March 2000 to December 2006: (a and b) precipitation and (c and d) near-surface air temperature.

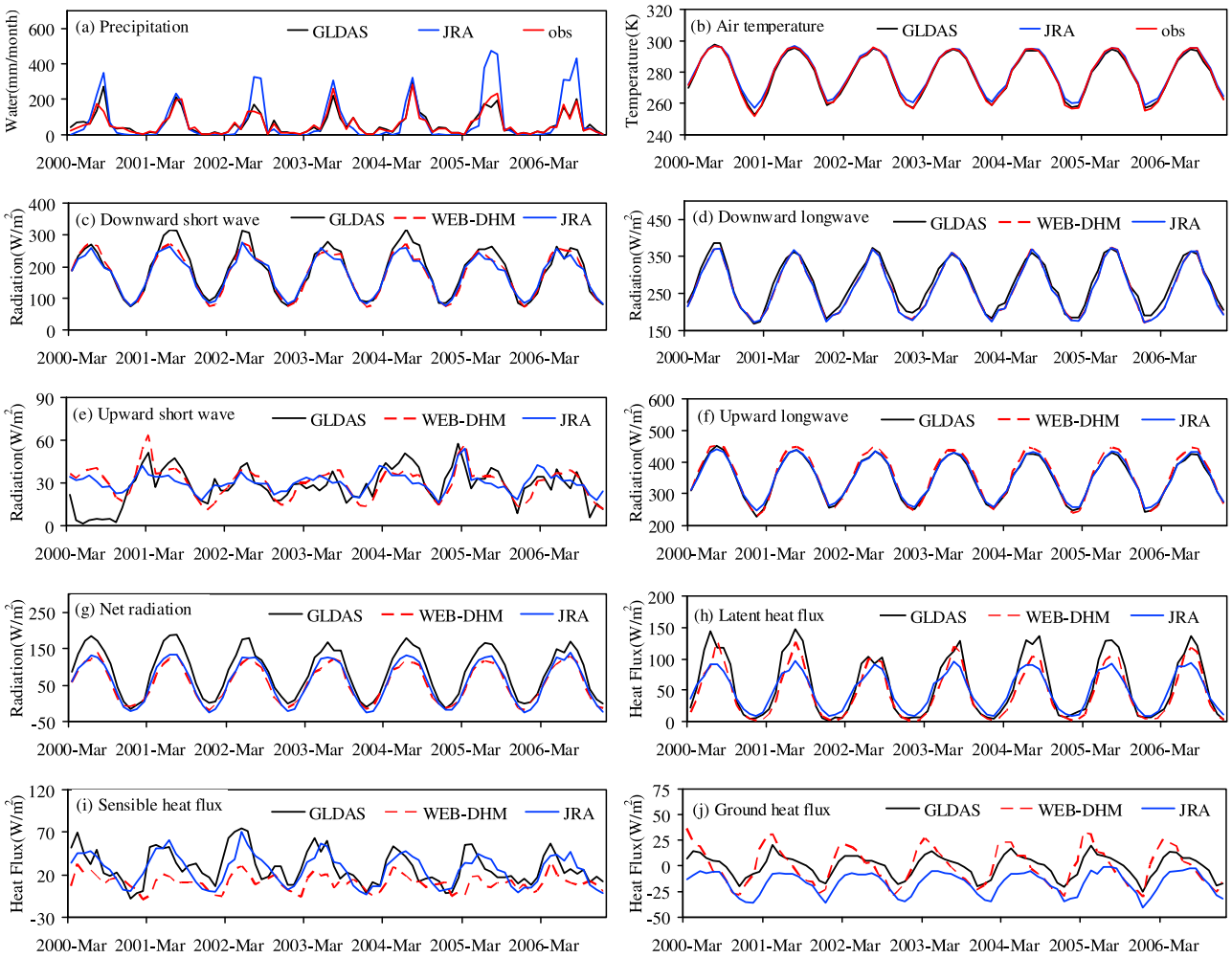

Figure 10. Comparison of monthly values averaged at the whole basin among the WEB-DHM simulations, the GLDAS/Noah, and the JRA-25 product from March 2000 to December 2006: (a) precipitation; (b) near-surface air temperature; (c) downward shortwave radiation; (d) downward longwave radiation; (e) upward shortwave radiation; (f) upward longwave radiation; (g) net radiation; (h) latent heat flux; (i) sensible heat flux and (j) ground heat flux.

[43] Figure 10d shows the level of downward longwave radiation ($R_{lw,d}$) for GLDAS, WEB-DHM and JRA-25. The $R_{lw,d}$ is consistent among the three models, where the WEB-DHM uses the same data as JRA-25. Figures 11g and 11h show that R is as high as 0.9910 between GLDAS and the WEB-DHM.

3.2.3. Summary

[44] The objective of section 3.2 was to evaluate the accuracy of the GLDAS atmospheric forcing data (P, T_{air}, $R_{sw,d}$, and $R_{lw,d}$) comparing with JRA-25 (P, T_{air}, $R_{sw,d}$, and $R_{lw,d}$), and in situ (P, T_{air}, and $R_{sw,d}$) observations. In summary, the P, T_{air} (daily and monthly) and $R_{lw,d}$ of GLDAS agreed well with observed P, T_{air} and JRA-25 $R_{lw,d}$, while the GLDAS $R_{sw,d}$ (monthly) shown larger values compared with observed $R_{sw,d}$. In general, the GLDAS atmospheric forcing data show 3 advantages: (1) the high resolution of GLDAS product with temporal scale of 3-h and spatial scale of 0.25-degree; (2) the reliability of GLDAS forcing especially its precipitation (both daily and monthly); and (3) GLDAS is available at the global scale. These findings are particularly important for ungauged or poorly gauged river basins, due to their forcing data problems [e.g., *Qian et al.*, 2006].

3.3. Comparing GLDAS/Noah Outputs With JRA-25 and WEB-DHM

3.3.1. Daily Scale

[45] Figure 12 shows the daily LST and ET as time series and scatterplots. In sections 3.3.1 and 3.3.2, the MBE and RMSE are calculated by comparing WEB-DHM (or JRA-25) simulations with GLDAS/Noah outputs. It should be mentioned that these statistical values (MBE and RMSE) do not necessarily represent model errors, but examine the differences among different models' outputs.

[46] Daily LSTs (Figure 12a) obtained with GLDAS/Noah and the WEB-DHM are quite comparable, with R, MBE and RMSE being 0.9764, 1.26 K and 3.59 K, respectively (Figure 12c). The underestimation of LST peak values by GLDAS/Noah has been reported [*Yang et al.*, 2009a] and attributed to overestimation of the thermal roughness length ($z0h$; discussion of z_{0h} is given in section 3.3.2).

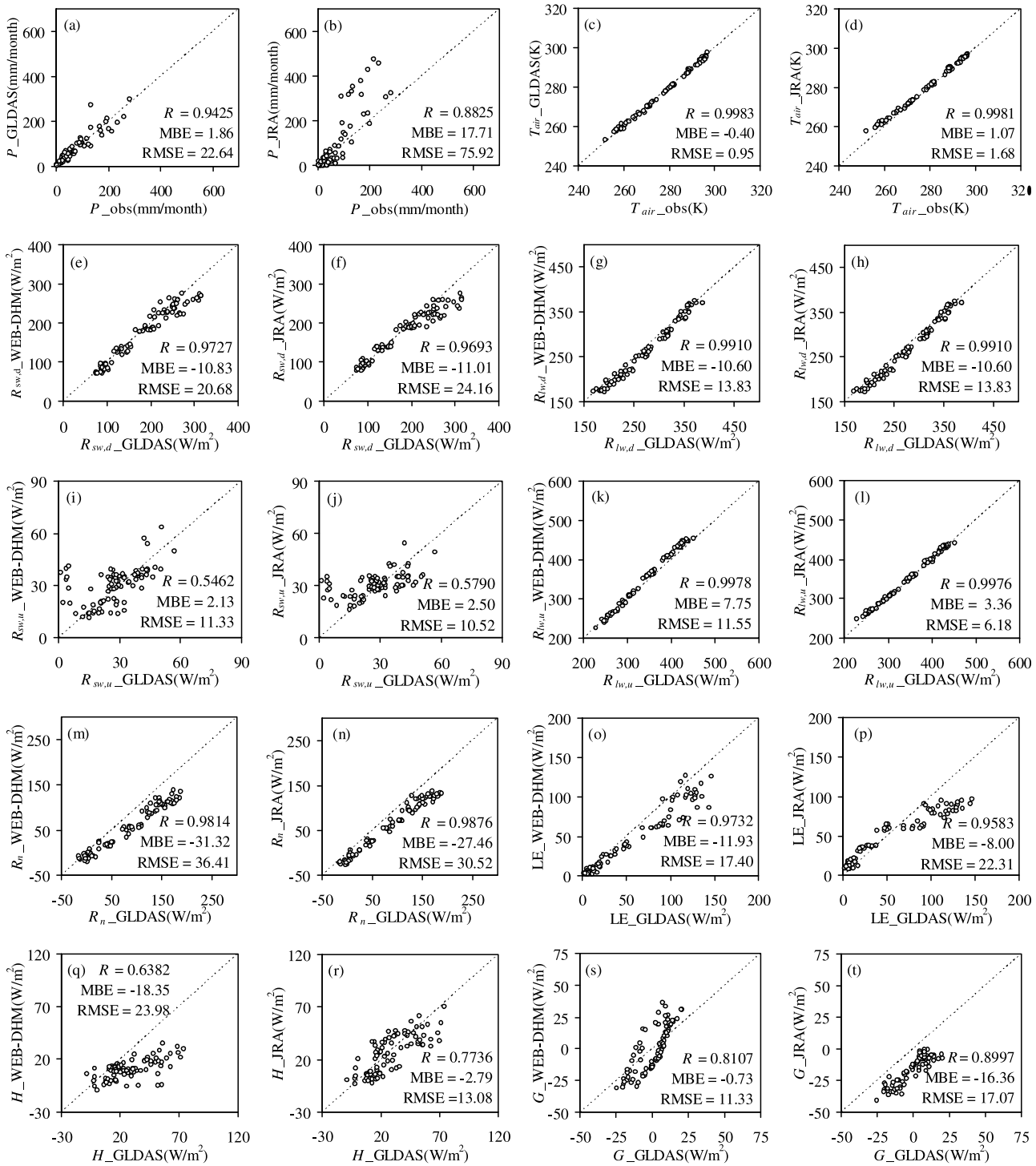

Figure 11. Same as Figure 10, but in scatterplots. MBE and RMSE are calculated by comparing the *y* axis with the *x* axis values.

[47] As shown in Figure 12b, the daily ET variation is in good agreement among the three models with *R* being 0.9121 between WEB-DHM and GLDAS/Noah and 0.9110 between JRA-25 and GLDAS/Noah. However, it is greater in summer for GLDAS/Noah than for the WEB-DHM and JRA-25. The MBE is −0.39 mm/day between WEB-DHM and GLDAS/Noah and −0.28 mm/day between JRA-25 and GLDAS/Noah, respectively. Different net radiations are mainly responsible for these differences, which is elaborated on in the following section on latent heat flux.

3.3.2. Monthly Scale

[48] Figures 10e–10j and 11i–11t show the model output variables of GLDAS/Noah, the WEB-DHM and JRA-25 as time series and scatterplots, respectively. The output variables include upward shortwave radiation ($R_{sw,u}$), upward

Table 3. Statistics of $R_{sw,d}$ Between the GLDAS and in Situ Observations for Warm Season (WS) and Cold Season (CS) From March 2000 to December 2006

	CS (April – August)		WS (September – March)	
Meteorological Gauge	MBE	RMSE	MBE	RMSE
Changchun (W/m^2)	15.14	19.75	56.94	60.56
Shenyang (W/m^2)	25.63	28.13	65.43	70.56
Yanji (W/m^2)	19.61	22.94	52.66	57.98
Basin average (W/m^2)	16.95	20.54	54.61	59.45

longwave radiation ($R_{lw,u}$), net radiation (R_n), latent heat flux (LE), sensible heat flux (H) and ground heat fluxes (G).

[49] The upward shortwave radiation ($R_{sw,u}$, Figure 10e) is well reproduced although there are slight biases. The extremely low values for GLDAS/Noah initially (Figure 10e) is mainly due to the uncertainty of albedo. R (Figures 11i and 11j) increases to 0.7773 and 0.7153 (data not shown) when the data for 2000, which are improperly initialized, are exempted. MBE decreases to −0.67 W/m^2 and −0.01 W/m^2 concurrently (data not shown). These results indicate that $R_{sw,u}$ can be estimated well by all three models.

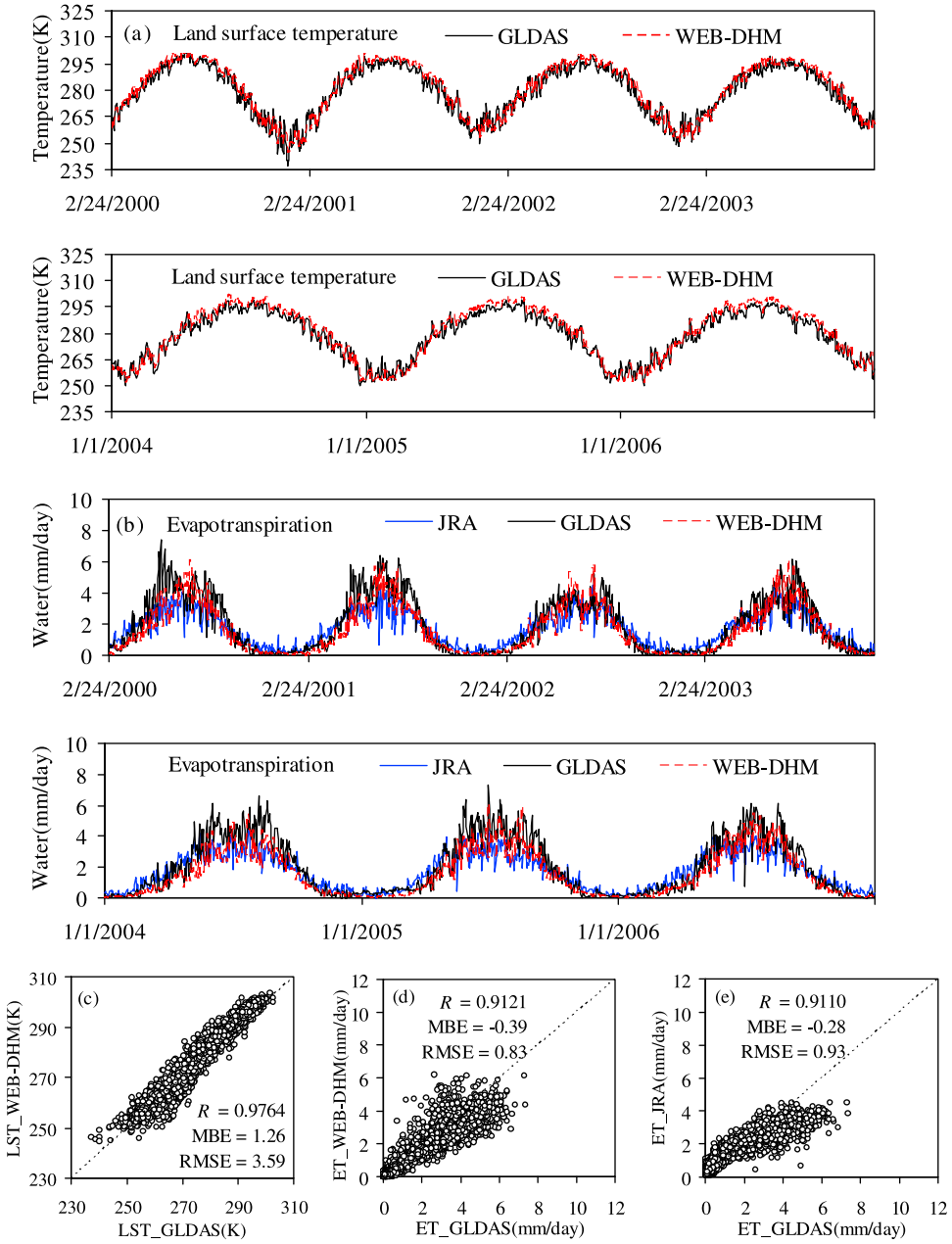

Figure 12. Comparison of daily values averaged at the whole basin, among the WEB-DHM simulations, the GLDAS/Noah, and the JRA-25 product from March 2000 to December 2006: (a) land surface temperature (time series); (b) evapotranspiration (time series); (c) land surface temperature (scatterplots), and (d, e) evapotranspiration (scatterplots).

[50] The upward longwave radiation ($R_{lw,u}$, Figure 10f) is well simulated by all three models, except that the WEB-DHM gives slightly higher values for summer. Both the WEB-DHM and the Noah LSM calculate $R_{lw,u}$ from the LST using the Stefan–Boltzmann law and the two models assume blackbody radiation (i.e., $\varepsilon = 1$) [*Hong and Kim*, 2008]. Therefore, the higher level of $R_{lw,u}$ of the WEB-DHM is mainly due to its higher LSTs (Figures 12a and 12c). The high R (0.9978 and 0.9976, Figures 11k and 11l) reveals that the three models reproduce the $R_{lw,u}$ variation fairly well.

[51] Figure 10g compares the net radiation (R_n) in the time series. There is distinctive divergence in summer with GLDAS/Noah giving a higher level than JRA-25 and the WEB-DHM. The higher level of $R_{sw,d}$ of GLDAS/Noah mostly accounts for this discrepancy. Although MBE and RMSE are as large as −31.32 W/m^2 and −27.46 W/m^2 (Figures 11m and 11n), R is quite high in both comparisons (0.9814 and 0.9876), indicating that all the three models capture the seasonal variations.

[52] Figure 10h compares latent heat flux (LE). There are conspicuous divisions for the wet seasons with GLDAS/Noah giving larger peak values than the WEB-DHM and JRA-25. It has been reported that R_n plays a more important role than soil moisture in controlling evaporation during wet seasons [*Yang et al.*, 2009a]. *Kato et al.* [2007] also pointed out that a wetter condition and more radiation input can lead to a wider possible range of LE. Therefore, the LE of GLDAS/Noah in summer is greater according to its higher level of R_n (Figure 10g). However, for dry seasons, ET is mainly controlled by soil surface resistance (r_{soil}) rather than net radiation [*Yang et al.*, 2009a]. r_{soil} is an empirical term to represent the impedance of the soil pores to exchanges of water vapor between the top layer soil and the immediately overlying air [*Sellers et al.*, 1996a; *van de Griend and Owe*, 1994]. Because all these models include r_{soil} [*Sellers et al.*, 1996a; *Betts et al.*, 1997; *Ek et al.*, 2003], the simulated phases of the monthly LE are similar among the three models in dry seasons. There is a typical drier case in 2002 (see Figure 5), and the comparison of LE in 2002 shows better consistency than comparisons for other years (Figure 10h). In general, the three estimations of LE reveal good agreements with R equal to 0.9732 between the WEB-DHM and the GLDAS/Noah and 0.9583 between the JRA-25 and the GLDAS/Noah (Figures 11o and 11p).

[53] Figure 10i shows the variation in the sensible heat flux (H). WEB-DHM gives lower values than GLDAS/Noah and JRA-25 but reproduces the seasonal variations fairly well. The MBE values are −18.35 W/m^2 and −2.79 W/m^2 for the WEB-DHM and JRA-25 comparing with GLDAS/Noah (Figures 11q and 11r). *Yang et al.* [2009a] and *Hong and Kim* [2010] also found larger H for Noah LSM comparing with SiB2 and observations.

[54] In the Noah LSM, the sensible heat flux (H) is calculated through the bulk heat transfer equation [*Chen et al.*, 1997]:

$$H = \rho C_P C_h |U_a| (\theta_s - \theta_a), \tag{7}$$

where ρ is the air density; C_p is the specific heat capacity of air at constant pressure; C_h is the surface exchange coefficient for heat; U_a is the wind speed; θ_a is the air potential temperature; θ_s is the corresponding variable at the surface.

[55] C_h is a crucial parameter which governs the total surface heat fluxes [*Chen and Zhang*, 2009; *Chen et al.*, 2010]. Recent studies [e.g., *Chen and Zhang*, 2009] show that the Noah LSM overestimates C_h (implying too efficient coupling) for short vegetation (e.g., crops, grass, shrubs, sparsely vegetated area) and underestimates it (implying insufficient coupling) for tall vegetation (e.g., forests). This problem is caused by the treatment of roughness length for heat (z_{0h}) (or thermal roughness length) in the Noah LSM. z_{0h} is the height at which the extrapolated air temperature equals the actual surface skin (radiative) temperature and it plays a critical role in estimating the total surface heat fluxes from the surface to the atmosphere [e.g., *Verhoef et al.*, 1997; *Yang et al.*, 2008; *Chen and Zhang*, 2009]. Noah LSM uses *Zilitinkevich*'s [1995] scheme to calculate z_{0h}, and this scheme possibly overestimates z_{0h} in bare-soil or sparsely vegetated area [e.g., *LeMone et al.*, 2008; *Yang et al.*, 2008]. According to Monin-Obukhov similarity theory based stability functions of Paulson [see *Paulson*, 1970; *Chen et al.*, 1997], the uncertainty of z_{0h} results in uncertainty of C_h.

[56] In the study basin (Figure 4c), most of the region (around 60%) is covered by agriculture or C3 grassland (short vegetation) which implies the C_h of Noah is possibly overestimated (z_{0h} overestimated). A higher C_h in equation (7) enhances the transport of heat H (Figures 10i, 11q, and 11r) from the surface to the atmosphere, resulting in a decrease in LST (Figures 12a and 12c) [*LeMone et al.*, 2008].

[57] All three models reproduce similar monthly variations in ground heat fluxes (G, Figure 10j), with the WEB-DHM giving a larger amplitude. However, the annual mean G of GLDAS/Noah is nearly the same as that of the WEB-DHM (Figure 11s). The same results were obtained by *Hong and Kim* [2010] when comparing SiB2 and Noah LSM for the Tibetan plateau, which is due to SiB2 having a smaller soil heat capacity than Noah. Consequently, the range of G is wider in the WEB-DHM than that in GLDAS/Noah. Meanwhile, the lower peak value of LSTs (Figure 12a) in GLDAS/Noah would directly result in lower G, which is also consistent with the higher H (Figure 10i).

[58] Soil moisture (SM) is a highly variable parameter in semiarid regions and plays a major role in determining ET and surface temperatures through modification of the surface energy budget [*Yang and Koike*, 2008; *Gottschalck et al.*, 2005; *Rüdiger et al.*, 2009]. Consequently, it is important to diagnose the accuracy of the simulated SM. Figure 13 shows the monthly mean surface SM obtained from WEB-DHM simulations and in situ observations in summer season from 2000 to 2006. The in situ data were observed at Huadian station (Figure 2b), while the WEB-DHM simulations were executed at the model grid (1 km resolution) which covered this station. The simulated SM agrees fairly well with the observed ones with a slightly negative bias (−0.017 m^3/m^3).

3.3.3. Summary

[59] The objective of section 3.3 was to investigate the performance of GLDAS/Noah simulated LST, ET, $R_{sw,u}$, $R_{lw,u}$, R_n, LE, H and G by comparing with the simulations obtained from WEB-DHM and JRA-25. First, the monthly

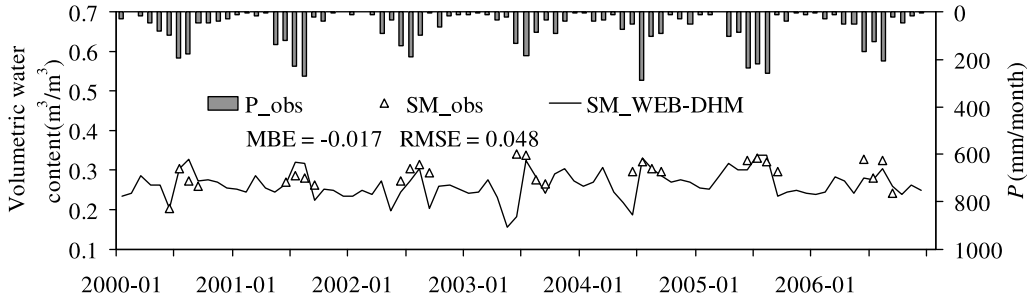

Figure 13. Comparison of monthly surface soil moisture (top 10 cm) between the WEB-DHM simulation and the ground-based observation at Huadian Station from 2000 to 2006 (summer). The observed monthly precipitation is also given for reference.

R_n and LE (and daily ET) estimated by GLDAS/Noah in wet seasons were higher than those estimated by the WEB-DHM and JRA-25. Second, the peak values of GLDAS/Noah daily LSTs (monthly H) were slightly lower (higher) than WEB-DHM simulations. Third, the $R_{sw,u}$ and $R_{lw,u}$ were well estimated by all three models. Fourth, GLDAS/Noah gave smaller range of monthly G values than the WEB-DHM. The performance of the simulated water and energy fluxes by GLDAS/Noah would provide references for other semi-arid river basins.

3.4. Application of the GLDAS Forcing Data in Driving Basin Scale Distributed Hydrological Model

[60] In the above study, WEB-DHM was driven by the observation-based meteorological data, which may be unavailable or very scarce in many river basins (e.g., ungauged basins). It will be helpful if the GLDAS forcing data could be applicable to the basin–scale studies as the inputs for distributed hydrological models (DHMs). Therefore, as a demonstration, this section we will examine the applicability of GLDAS global forcing data to the study basin by driving the WEB-DHM using GLDAS forcing data.

3.4.1. Experiment Results

[61] Table 4 lists the monthly $R_{sw,d}$ of GLDAS and in situ observation and their differences. Two conclusions can be drawn from this comparison: (1) GLDAS overestimates $R_{sw,d}$ for each month; (2) the largest differences happen from April to August. Due to the overestimation of $R_{sw,d}$ for GLDAS product, it is necessary to correct the GLDAS $R_{sw,d}$ by using in situ observations. Two different correction functions are derived in warm season (WS, from April to August) and cold season (CS, from September to March), respectively.

$$\text{Warm season}: R_{sw,d,rev} = 0.7823 \times R_{sw,d}, \tag{8}$$

$$\text{Cold season}: R_{sw,d,rev} = 0.8563 \times R_{sw,d}, \tag{9}$$

where $R_{sw,d}$ and $R_{sw,d,rev}$ are the original and revised GLDAS daily downward shortwave radiation, respectively. Figure 14a reveals the basin average monthly mean corrected $R_{sw,d}$ compared with in situ observations and the original $R_{sw,d}$. $R_{sw,d}$ improved significantly after correction especially in warm seasons.

[62] Figure 14b shows the daily Q at Wudaogou station (Figure 2b), simulated by using the GLDAS corrected $R_{sw,d}$ and original $R_{sw,d}$ compared with ground-based observation. NS coefficient improves from 0.540 to 0.629 after $R_{sw,d}$ is corrected. Meanwhile, RB changes from negative value (−17.33%) to positive value (17.64%). This is because the lower $R_{sw,d}$ leads to lower ET and results in larger Q after $R_{\mathrm{sw,d}}$ is corrected.

[63] Figure 14c compares monthly mean discharge and ET by using the original GLDAS $R_{sw,d}$ and revised $R_{sw,d}$. ET shows larger value than WEB-DHM simulation while Q is underestimated compared with ground-based observation when using original $R_{sw,d}$. ET decreases significantly after revising the $R_{sw,d}$, while Q increases. The Q simulated by using revised $R_{sw,d}$ is more comparable to measured streamflow than using GLDAS original $R_{sw,d}$ with NS coefficient improves from 0.695 to 0.839.

3.4.2. Summary

[64] The objective of section 3.4 was to evaluate the applicability of the GLDAS atmospheric forcing data (P, $R_{sw,d}$, $R_{lw,d}$, T_{air}, Q_a, P_s, U and V) in simulating basin scale water cycles by using WEB-DHM. In summary, the Q (ET) simulated by using original GLDAS forcing data was underestimated (overestimated) because the larger $R_{sw,d}$ caused larger ET (lower Q). After revising the $R_{sw,d}$ by using 2 simple linear equations (equations (8) and (9)), the basin-integrated Q and ET were reproduced reasonably well. This part has demonstrated the feasibility of the applications of WEB-DHM fed with GLDAS forcing into different river basins.

4. Conclusions

[65] The accurate atmospheric data with high-resolution (both spatial and temporal) are essential for basin scale water and energy studies. However, the high-resolution, realistic atmospheric data are usually not available from observations [*Qian et al.*, 2006]. In order to solve this problem, this paper aimed to evaluate and apply GLDAS/Noah (0.25-degree, 3-h) for basin scale water and energy cycle studies. This goal was realized through demonstrating four supporting objectives. The major findings (corresponding to 4 objectives) from this study are as follows.

[66] First, in order to validate a basin scale DHM in simulating water and energy budget, for the evaluation and application of the fine-resolution global data set, WEB-DHM was carefully validated by using measured streamflows and MODIS/Terra LSTs. The discharges at 2 major stations simulated by the WEB-DHM agreed well with in situ observations with RB of −6.37% and 5.60%. The model

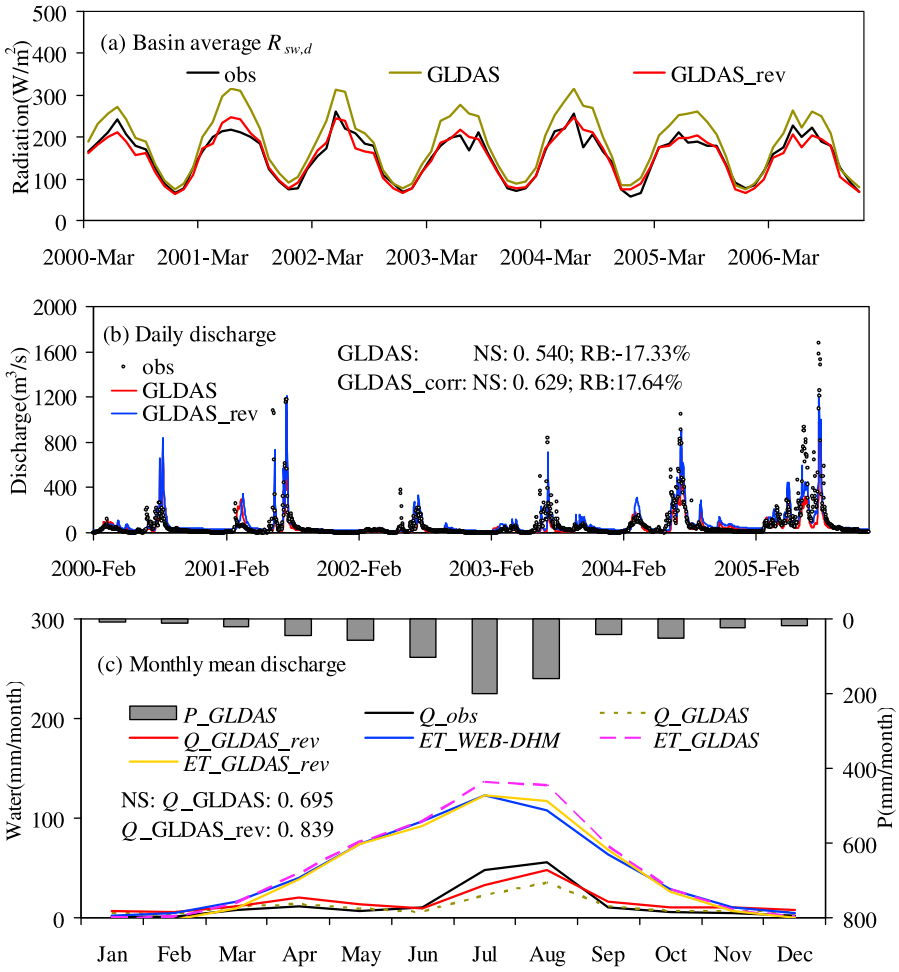

Figure 14. The correction results of GLDAS downward shortwave radiation ($R_{sw,d}$): (a) the corrected monthly $R_{sw,d}$ averaged at the whole basin compared with in situ observation and original GLDAS $R_{sw,d}$ from March 2000 to December 2006, (b) simulated daily discharge (Q), and (c) inter-annual mean monthly Q, and evapotranspiration (ET) by using the original and the corrected GLDAS/Noah forcing data for the Wudaogou subbasin from February 2000 to December 2005.

also reproduced LSTs well in terms of both the time series and seasonal spatial distribution when compared with MODIS/Terra V5 LSTs despite the WEB-DHM giving slightly larger peak values. From this validation, it was concluded that the WEB-DHM is able to predict water and energy fluxes accurately over the semi-arid river basin (the upper Second Songhua River basin).

[67] Second, in order to evaluate the accuracy of the GLDAS atmospheric forcing data (P, T_{air}, $R_{sw,d}$, and $R_{lw,d}$), they were compared with in situ observations (P, T_{air}, $R_{sw,d}$), and JRA-25 product (P, T_{air}, $R_{sw,d}$, and $R_{lw,d}$). The P of GLDAS was found to be more accurate on a monthly scale than on a daily scale by comparing with ground-based observations, but in both cases, GLDAS performed better than JRA-25, which has coarse spatial resolution. Good

Table 4. Comparison of Monthly $R_{sw,d}$ Between GLDAS/Noah and in Situ Observation From 2000 to 2006[a]

Month	Jan	Feb	Mar	Apr	May	Jun
GLDAS/Noah (W/m^2)	82.88	119.68	172.62	212.33	245.26	246.82
Observation (W/m^2)	66.87	105.48	142.25	164.30	193.02	190.34
Difference (W/m^2)	16.02	14.20	30.37	**48.03**	**52.25**	**56.48**
Month	Jul	Aug	Sep	Oct	Nov	Dec
GLDAS/Noah (W/m^2)	229.59	210.35	176.58	124.92	84.77	71.39
Observation (W/m^2)	172.87	168.59	152.30	109.31	75.02	60.62
Difference (W/m^2)	**56.72**	**41.76**	24.28	15.61	9.75	10.77

[a]The bold values from April to August mean relatively larger differences than those for other months.

correlation was found for T_{air} when comparing GLDAS to ground-based observations and JRA-25 on both daily and monthly scales. GLDAS also had good performance for monthly $R_{lw,d}$. However, GLDAS gave a higher level for monthly $R_{sw,d}$ than the in situ observation.

[68] Third, in order to analyze the performance of the GLDAS/Noah outputs (LST, ET, $R_{sw,u}$, $R_{lw,u}$, R_n, LE, H, and G), they were compared with WEB-DHM simulations and JRA-25 product. Because the roughness length for heat (z_{0h}) in Noah LSM was improper treated [e.g., *LeMone et al.*, 2008; *Yang et al.*, 2008], Noah overestimated C_h (implying too efficient coupling) for short vegetations (e.g., crops, sparsely vegetated area) [e.g., *Chen and Zhang*, 2009] which are the dominant land use type in the study basin. A higher C_h enhanced the transport of heat H from the surface to the atmosphere, resulting in a decrease in LST [*LeMone et al.*, 2008]. Therefore, GLDAS/Noah gave higher monthly H than the WEB-DHM and JRA-25, while the peak values of GLDAS/Noah daily LSTs were lower than WEB-DHM. Because of the lower LST peaks for the GLDAS/Noah, the level of GLDAS/Noah monthly $R_{lw,u}$ was higher in summer, while the monthly $R_{sw,u}$ was well estimated by all three models. The higher level of monthly $R_{sw,d}$ of GLDAS/Noah resulted in R_n being at a slightly higher level than that for the WEB-DHM and JRA-25. Daily ET and monthly LE estimated by GLDAS/Noah in wet seasons were higher than those estimated by the WEB-DHM and JRA-25 owing to the higher level of R_n. GLDAS/Noah gave a smaller range of monthly G values than the WEB-DHM owing to the greater soil heat capacity used in Noah and a lower peak value of LSTs in GLDAS/Noah than in the WEB-DHM. The monthly mean surface 10 cm SM estimated by WEB-DHM performed well compared with in situ observations at Huadian station.

[69] Finally, in order to evaluate the applicability of GLDAS global forcing data (P, $R_{sw,d}$, $R_{lw,d}$, T_{air}, near-surface specific humidity, surface pressure and wind speed) for basin scale water resources management, the WEB-DHM was driven by using original and revised GLDAS forcing data. Because GLDAS overestimated $R_{sw,d}$, the ET was overestimated while discharge was underestimated when using original GLDAS forcing data. The performance of simulated ET and discharge were improved when revise the $R_{sw,d}$ by using simple linear equations for warm and cold seasons, respectively.

[70] These results confirm the capability of WEB-DHM and GLDAS/Noah in modeling basin-wide water and energy budget in semiarid basin. Meanwhile, GLDAS can give reliable fine-resolution global atmospheric forcing data which are essential for WEB-DHM (or other DHMs). The combination of GLDAS with WEB-DHM (or other DHMs) would benefit more basins around the world (e.g., for water resources management). Given the increasing world wide water resources problems [*Intergovernmental Panel on Climate Change*, 2007], further efforts are needed to deepen this combination.

[71] **Acknowledgments.** The authors are grateful to three reviews whose comments are helpful to improve the quality of this paper. The authors also gratefully acknowledge financial support provided by the China Scholarship Council. This study was supported by National Natural Science Foundation of China (grant 50809010). Parts of this work were also supported by grants from the Ministry of Education, Culture, Sports, Science and Technology of Japan. GLDAS data used in this study were acquired as part of a mission of NASA's Earth Science Division and archived and distributed by the Data and Information Services Center of Goddard Earth Sciences. The authors sincerely thank Hiroko Kato Beaudoing, who provided guidance in extracting GLDAS data. The JRA-25 data sets used in this study are from the JRA-25 long-term reanalysis cooperative research project carried out by the Japan Meteorological Agency and the Central Research Institute of Electric Power Industry.

References

Asian Development Bank (2002), Report and recommendation of the president to the board of directors on a proposed loan to the People's Republic of China for the Songhua River flood management sector project, *Rep. RRP: PRC 33437*, Manila.

Bertoldi, G., C. Notarnicola, G. Leitinger, S. Endrizzi, M. Zebisch, S. D. Chiesa, and U. Tappeiner (2010), Topographical and ecohydrological controls on land surface temperature in an alpine catchment, *Ecohydrology*, *3*(2), 189–204, doi:10.1002/eco.129.

Betts, A. K., F. Chen, K. E. Mitchell, and Z. I. Janjic (1997), Assessment of the land surface and boundary layer models in two operational versions of the NCEP Eta model using FIFE data, *Mon. Weather Rev.*, *125*, 2896–2916, doi:10.1175/1520-0493(1997)125<2896:AOTLSA>2.0.CO;2.

Bowling, L. C., et al. (2003), Simulation of high-latitude hydrological processes in the Torne–Kalix basin: PILPS Phase 2(e): 1: Experiment description and summary intercomparisons, *Global Planet. Change*, *38*(1–2), 1–30, doi:10.1016/S0921-8181(03)00003-1.

Briegleb, B. P. (1992), Delta-Eddington approximation for solar radiation in the NCAR Community Climate Model, *J. Geophys. Res.*, *97*(D7), 7603–7612, doi:10.1029/92JD00291.

Chen, F., and J. Dudhia (2001), Coupling an advanced land-surface/hydrology model with the Penn State/NCAR MM5 modeling system. Part I: Model description and implementation, *Mon. Weather Rev.*, *129*(4), 569–585, doi:10.1175/1520-0493(2001)129<0569:CAALSH>2.0.CO;2.

Chen, F., and Y. Zhang (2009), On the coupling strength between the land surface and the atmosphere: From viewpoint of surface exchange coefficients, *Geophys. Res. Lett.*, *36*, L10404, doi:10.1029/2009GL037980.

Chen, F., K. Mitchell, J. Schaake, Y. Xue, H.-L. Pan, V. Koren, Q. Y. Duan, M. Ek, and A. Betts (1996), Modeling of land surface evaporation by four schemes and comparison with FIFE observations, *J. Geophys. Res.*, *101*(D3), 7251–7268, doi:10.1029/95JD02165.

Chen, F., Z. Janjic, and K. Mitchell (1997), Impact of atmospheric surface-layer parameterizations in the new land-surface scheme of the NCEP Mesoscale Eta Model, *Boundary Layer Meteorol.*, *85*, 391–421, doi:10.1023/A:1000531001463.

Chen, Y., K. Yang, D. Zhou, J. Qin, and X. Guo (2010), Improving the Noah land surface model in arid regions with an appropriate parameterization of the thermal roughness length, *J. Hydrometeorol.*, *11*, 995–1006, doi:10.1175/2010JHM1185.1.

Coakley, J. A., R. D. Cess, and F. B. Yurevich (1983), The effect of tropospheric aerosols on the Earth's radiation budget: A parameterization for climate models, *J. Atmos. Sci.*, *40*(1), 116–138, doi:10.1175/1520-0469(1983)040<0116:TEOTAO>2.0.CO;2.

Cosgrove, B. A., et al. (2003), Real-time and retrospective forcing in the North American Land Data Assimilation System (NLDAS) project, *J. Geophys. Res.*, *108*(D22), 8842, doi:10.1029/2002JD003118.

Dai, Y., et al. (2003), The Common Land Model (CLM), *Bull. Am. Meteorol. Soc.*, *84*(8), 1013–1023, doi:10.1175/BAMS-84-8-1013.

Derber, J. C., D. F. Parrish, and S. J. Lord (1991), The new global operational analysis system at the National Meteorological Center, *Weather Forecast.*, *6*, 538–547, doi:10.1175/1520-0434(1991)006<0538:TNGOAS>2.0.CO;2.

Dirmeyer, P. A., A. J. Dolman, and N. Sato (1999), The pilot phase of the Global Soil Wetness Project, *Bull. Am. Meteorol. Soc.*, *80*(5), 851–878, doi:10.1175/1520-0477(1999)080<0851:TPPOTG>2.0.CO;2.

Ek, M. B., K. E. Mitchell, Y. Lin, E. Rogers, P. Grunmann, V. Koren, G. Gayno, and J. D. Tarpley (2003), Implementation of Noah land surface model advances in the National Centers for Environmental Prediction operational mesoscale Eta model, *J. Geophys. Res.*, *108*(D22), 8851, doi:10.1029/2002JD003296.

Food and Agriculture Organization (FAO) (2003), Digital soil map of the world and derived soil properties, land and water digital media series [CD-ROM], rev. 1, Rome.

Gottschalck, J., J. Meng, M. Rodell, and P. Houser (2005), Analysis of multiple precipitation products and preliminary assessment of their impact on Global Land Data Assimilation System (GLDAS) land surface states, *J. Hydrometeorol.*, *6*(5), 573–598, doi:10.1175/JHM437.1.

Henderson-Sellers, A., A. J. Pitman, P. K. Love, P. Irannejad, and T. H. Chen (1995), The Project for Intercomparison of Land–surface Parameterization Schemes (PILPS)-Phase-2 and Phase-3, *Bull. Am. Meteorol. Soc.*, *76*(4), 489–503, doi:10.1175/1520-0477(1995)076<0489:TPFIOL>2.0.CO;2.

Hong, J., and J. Kim (2008), Simulation of surface radiation balance on the Tibetan Plateau, *Geophys. Res. Lett.*, *35*, L08814, doi:10.1029/2008GL033613.

Hong, J., and J. Kim (2010), Numerical study of surface energy partitioning on the Tibetan plateau: Comparative analysis of two biosphere models, *Biogeosciences*, *7*(2), 557–568, doi:10.5194/bg-7-557-2010.

Idso, S. (1981), A set of equations for the full spectrum and 8- to 14-μm and 10.5- to 12.5-μm thermal radiation from cloudless skies, *Water Resour. Res.*, *17*(2), 295–304, doi:10.1029/WR017i002p00295.

Intergovernmental Panel on Climate Change (2007), *Climate Change 2007: Climate Change Impacts, Adaptation and Vulnerability, Summary for Policymakers*, Cambridge Univ. Press, Cambridge, U. K.

Japan Meteorological Agency (JMA) (2007), Outline of the operational forecast and analysis system of the Japan Meteorological Agency, appendix to WMO technical progress report on the global data-processing and forecasting system and numerical weather prediction, Tokyo. [Available at http://www.jma.go.jp/jma/jma-eng/jma-center/nwp/outline-nwp/index.htm]

Jaranilla-Sanchez, P. A., L. Wang, and T. Koike (2011), Modeling the hydrologic responses of the Pampangga River Basin, Philippines: A quantitative approach for identifying droughts, *Water Resour. Res.*, *47*, W03514, doi:10.1029/2010WR009702.

Joseph, J. H., W. J. Wiscombe, and J. A. Weinman (1976), The delta-Eddington approximation for radiative flux transfer, *J. Atmos. Sci.*, *33*(12), 2452–2459, doi:10.1175/1520-0469(1976)033<2452:TDEAFR>2.0.CO;2.

Kato, H., M. Rodell, F. Beyrich, H. Cleugh, E. van Gorsel, H. Liu, and T. P. Meyers (2007), Sensitivity of land surface simulations to model physics, parameters, and forcings, at four CEOP sites, *J. Meteorol. Soc. Jpn.*, *85A*, 187–204, doi:10.2151/jmsj.85A.187.

Koren, V., J. Schaake, K. Mitchell, Q.-Y. Duan, F. Chen, and J. M. Baker (1999), A parameterization of snowpack and frozen ground intended for NCEP weather and climate models, *J. Geophys. Res.*, *104*(D16), 19,569–19,585, doi:10.1029/1999JD900232.

Koster, R. D., and M. J. Suarez (1992a), A comparative analysis of two land surface heterogeneity representations, *J. Clim.*, *5*, 1379–1390, doi:10.1175/1520-0442(1992)005<1379:ACAOTL>2.0.CO;2.

Koster, R. D., and M. J. Suarez (1992b), Modeling the land surface boundary in climate models as a composite of independent vegetation stands, *J. Geophys. Res.*, *97*(D3), 2697–2715, doi:10.1029/91JD01696.

Koster, R. D., M. J. Suarez, A. Ducharne, M. Stiglitz, and P. Kumar (2000), A catchment-based approach to modeling land surface processes in a GCM: 1. Model structure, *J. Geophys. Res.*, *105*(D20), 24,809–24,822, doi:10.1029/2000JD900327.

Koster, R. D., M. J. Suarez, P. Liu, U. Jambor, A. Berg, M. Kistler, R. Reichle, M. Rodell, and J. Famiglietti (2004), Realistic initialization of land surface states: Impacts on subseasonal forecast skill, *J. Hydrometeorol.*, *5*(6), 1049–1063, doi:10.1175/JHM-387.1.

Kumar, S. V., et al. (2006), Land information system: An interoperable framework for high resolution land surface modeling, *Environ. Model. Softw.*, *21*(10), 1402–1415, doi:10.1016/j.envsoft.2005.07.004.

LeMone, M., M. Tewari, F. Chen, J. Alfieri, and D. Niyogi (2008), Evaluation of the Noah land surface model using data from a fair-weather IHOP_2002 day with heterogeneous surface fluxes, *Mon. Weather Rev.*, *136*, 4915–4941, doi:10.1175/2008MWR2354.1.

Liang, X., D. P. Lettenmaier, E. F. Wood, and S. J. Burges (1994), A simple hydrologically based model of land surface water and energy fluxes for GSMs, *J. Geophys. Res.*, *99*(D7), 14,415–14,428, doi:10.1029/94JD00483.

Luo, L., et al. (2003), Validation of the North American Land Data Assimilation System (NLDAS) retrospective forcing over the southern Great Plains, *J. Geophys. Res.*, *108*(D22), 8843, doi:10.1029/2002JD003246.

Mitchell, K. E., et al. (2004), The multi-institution North American Land Data Assimilation System (NLDAS): Utilizing multiple GCIP products and partners in a continental distributed hydrological modeling system, *J. Geophys. Res.*, *109*, D07S90, doi:10.1029/2003JD003823.

Myneni, R. B., R. R. Nemani, and S. W. Running (1997), Algorithm for the estimation of global land cover, LAI and FPAR based on radiative transfer models, *IEEE Trans. Geosci. Remote Sens.*, *35*, 1380–1393, doi:10.1109/36.649788.

Nash, J. E., and J. V. Sutcliffe (1970), River flow forecasting through conceptual models part I—A discussion of principles, *J. Hydrol.*, *10*(3), 282–290, doi:10.1016/0022-1694(70)90255-6.

Onogi, K., et al. (2007), The JRA-25 reanalysis, *J. Meteorol. Soc. Jpn.*, *85*(3), 369–432, doi:10.2151/jmsj.85.369.

Parton, W. J., and J. A. Logan (1981), A model for diurnal variation in soil and air temperature, *Agric. Meteorol.*, *23*, 205–216, doi:10.1016/0002-1571(81)90105-9.

Paulson, C. A. (1970), The mathematical representation of wind speed and temperature profiles in the unstable atmospheric surface layer, *J. Appl. Meteorol.*, *9*, 857–861, doi:10.1175/1520-0450(1970)009<0857:TMROWS>2.0.CO;2.

Pietroniro, A., and E. D. Soulis (2003), A hydrology modeling framework for the Mackenzie GEWEX programme, *Hydrol. Processes*, *17*(3), 673–676, doi:10.1002/hyp.5104.

Qian, T., A. G. Dai, K. E. Trenberth, and K. W. Oleson (2006), Simulation of global land surface conditions from 1948 to 2004. Part I: Forcing data and evaluations, *J. Hydrometeorol.*, *7*, 953–975, doi:10.1175/JHM540.1.

Rigon, R., G. Bertoldi, and T. M. Over (2006), GEOtop: A distributed hydrological model with coupled water and energy budgets, *J. Hydrometeorol.*, *7*, 371–388, doi:10.1175/JHM497.1.

Rodell, M., et al. (2004a), The Global Land Data Assimilation System, *Bull. Am. Meteorol. Soc.*, *85*(3), 381–394, doi:10.1175/BAMS-85-3-381.

Rodell, M., J. S. Famiglietti, J. Chen, S. Seneviratne, P. Viterbo, S. Holl, and C. R. Wilson (2004b), Basin scale estimates of evapotranspiration using GRACE and other observations, *Geophys. Res. Lett.*, *31*, L20504, doi:10.1029/2004GL020873.

Rodell, M., P. R. Houser, A. A. Berg, and J. S. Famiglietti (2005), Evaluation of ten methods for initializing a land surface model, *J. Hydrometeorol.*, *6*(2), 146–155, doi:10.1175/JHM414.1.

Rüdiger, C., J.-C. Calvet, C. Gruhier, T. Holmes, R. De Jeu, and W. Wagner (2009), An intercomparison of ERS-Scat and AMSR-E soil moisture observations with model simulations over France, *J. Hydrometeorol.*, *10*, 431–447, doi:10.1175/2008JHM997.1.

Saavedra Valeriano, O. C., T. Koike, K. Yang, T. Graf, X. Li, L. Wang, and X. Han (2010), Decision support for dam release during floods using a distributed biosphere hydrological model driven by quantitative precipitation forecasts, *Water Resour. Res.*, *46*, W10544, doi:10.1029/2010WR009502.

Sellers, P. J., Y. Mintz, Y. C. Sud, and A. Dalcher (1986), A simple biosphere model (SiB) for use within general circulation models, *J. Atmos. Sci.*, *43*(6), 505–531, doi:10.1175/1520-0469(1986)043<0505:ASBMFU>2.0.CO;2.

Sellers, P. J., D. A. Randall, G. J. Collatz, J. A. Berry, C. B. Field, D. A. Dazlich, C. Zhang, G. D. Collelo, and L. Bounoua (1996a), A revised land surface parameterization (SiB2) for atmospheric GCMs, part I: Model formulation, *J. Clim.*, *9*(4), 676–705, doi:10.1175/1520-0442(1996)009<0676:ARLSPF>2.0.CO;2.

Sellers, P. J., S. O. Los, C. J. Tucker, C. O. Justice, D. A. Dazlich, G. J. Collatz, and D. A. Randall (1996b), A revised land surface parameterization (SiB2) for atmospheric GCMs, part II: The generation of global fields of terrestrial biophysical parameters from satellite data, *J. Clim.*, *9*, 706–737, doi:10.1175/1520-0442(1996)009<0706:ARLSPF>2.0.CO;2.

Sellers, P. J., et al. (1997), A modeling the exchanges of energy, water, and carbon between continents and the atmosphere, *Science*, *275*(5299), 502–509, doi:10.1126/science.275.5299.502.

Shapiro, R. (1972), Simple model for the calculation of the flux of solar radiation through the atmosphere, *Appl. Opt.*, *11*(4), 760–764, doi:10.1364/AO.11.000760.

Shrestha, M., L. Wang, T. Koike, Y. Xue, and Y. Hirabayashi (2010), Improving the snow physics of WEB-DHM and its point evaluation at the SnowMIP sites, *Hydrol. Earth Syst. Sci.*, *14*(12), 2577–2594, doi:10.5194/hess-14-2577-2010.

Syed, T. H., J. S. Famiglietti, M. Rodell, J. L. Chen, and C. R. Wilson (2008), Analysis of terrestrial water storage changes from GRACE and GLDAS, *Water Resour. Res.*, *44*, W02433, doi:10.1029/2006WR005779.

Tang, Q., T. Oki, S. Kanae, and H. Hu (2007), The influence of precipitation variability and partial irrigation within grid cells on a hydrological simulation, *J. Hydrometeorol.*, *8*, 499–512, doi:10.1175/JHM589.1.

van de Griend, A., and M. Owe (1994), Bare soil surface resistance to evaporation by vapor diffusion under semiarid conditions, *Water Resour. Res.*, *30*(2), 181–188, doi:10.1029/93WR02747.

Verhoef, A., H. A. R. De Bruin, and B. J. J. M. Van Den Hurk (1997), Some practical notes on the parameter kB^{-1} for sparse vegetation, *J. Appl. Meteorol.*, *36*, 560–572, doi:10.1175/1520-0450(1997)036<0560:SPNOTP>2.0.CO;2.

Wan, Z. M. (2008), New refinements and validation of the MODIS land-surface temperature/emissivity products, *Remote Sens. Environ.*, *112*(1), 59–74, doi:10.1016/j.rse.2006.06.026.

Wang, A., and X. Zeng (2011), Sensitivities of terrestrial water cycle simulations to the variations of precipitation and air temperature in China, *J. Geophys. Res.*, *116*, D02107, doi:10.1029/2010JD014659.

Wang, L., T. Koike, K. Yang, T. J. Jackson, R. Bindlish, and D. W. Yang (2009a), Development of a distributed biosphere hydrological model and its evaluation with the Southern Great Plains Experiments (SGP97 and SGP99), *J. Geophys. Res.*, *114*, D08107, doi:10.1029/2008JD010800.

Wang, L., T. Koike, K. Yang, and P. Yeh (2009b), Assessment of a distributed biosphere hydrological model against streamflow and MODIS land surface temperature in the upper Tone River Basin, *J. Hydrol.*, *377*(1–2), 21–34, doi:10.1016/j.jhydrol.2009.08.005.

Wang, L., T. Koike, D. W. Yang, and K. Yang (2009c), Improving the hydrology of the Simple Biosphere Model and its evaluation within the framework of a distributed hydrological model, *Hydrol. Sci. J.*, *54*(6), 989–1006, doi:10.1623/hysj.54.6.989.

Wang, L., Z. Wang, T. Koike, H. Yin, D. Yang, and S. He (2010a), The assessment of surface water resources for the semi-arid Yongding River Basin from 1956 to 2000 and the impact of land use change, *Hydrol. Processes*, *24*, 1123–1132, doi:10.1002/hyp.7566.

Wang, L., T. Koike, K. Yang, R. Jin, and H. Li (2010b), Frozen soil parameterization in a distributed biosphere hydrological model, *Hydrol. Earth Syst. Sci.*, *14*, 557–571, doi:10.5194/hess-14-557-2010.

Warrach, K., M. Stieglitz, H. Mengelkamp, and E. Raschke (2002), Advantages of a topographically controlled runoff simulation in a SVAT model, *J. Hydrometeorol.*, *3*, 131–148, doi:10.1175/1525-7541(2002)003<0131:AOATCR>2.0.CO;2.

Wigmosta, M. S., L. W. Vail, and D. P. Lettenmaier (1994), A distributed hydrology-vegetation model for complex terrain, *Water Resour. Res.*, *30*(6), 1665–1679, doi:10.1029/94WR00436.

Xie, P. P., and P. A. Arkin (1997), Global precipitation: A 17-year monthly analysis based on gauge observations, satellite estimates, and numerical model outputs, *Bull. Am. Meteorol. Soc.*, *78*, 2539–2558, doi:10.1175/1520-0477(1997)078<2539:GPAYMA>2.0.CO;2.

Xie, P. P., J. E. Janowiak, P. A. Arkin, R. Adler, A. Gruber, R. Ferraro, G. J. Huffman, and S. Curtis (2003), GPCP Pentad precipitation analyses: An experimental dataset based on gauge observations and satellite estimates, *J. Clim.*, *16*, 2197–2214, doi:10.1175/2769.1.

Xue, Y., P. J. Sellers, J. L. Kinter, and J. Shukla (1991), A simplified biosphere model for global climate studies, *J. Clim.*, *4*(3), 345–364, doi:10.1175/1520-0442(1991)004<0345:ASBMFG>2.0.CO;2.

Yang, D. W., S. Herath, and K. Musiake (2002), A hillslope-based hydrological model using catchment area and width functions, *Hydrol. Sci. J.*, *47*(1), 49–65, doi:10.1080/02626660209492907.

Yang, D. W., T. Koike, and H. Tanizawa (2004a), Application of a distributed hydrological model and weather radar observations for flood management in the upper Tone River of Japan, *Hydrol. Processes*, *18*(16), 3119–3132, doi:10.1002/hyp.5752.

Yang, D. W., C. Li, G. H. Ni, and H. P. Hu (2004b), Application of a distributed hydrological model to the Yellow River Basin [in Chinese], *Acta Geogr. Sin.*, *59*(1), 143–154.

Yang, K., and T. Koike (2008), Satellite monitoring of the surface water and energy budget in the Central Tibetan Plateau, *Adv. Atmos. Sci.*, *25*, 974–985, doi:10.1007/s00376-008-0974-8.

Yang, K., G. W. Huang, and N. Tamai (2001), A hybrid model for estimating global solar radiation, *Sol. Energy.*, *70*(1), 13–22, doi:10.1016/S0038-092X(00)00121-3.

Yang, K., T. Koike, and B. S. Ye (2006), Improving estimation of hourly, daily, and monthly solar radiation by importing global data sets, *Agric. For. Meteorol.*, *137*(1–2), 43–55, doi:10.1016/j.agrformet.2006.02.001.

Yang, K., T. Koike, H. Ishikawa, J. Kim, X. Li, H.-Z. Liu, S.-M. Liu, Y.-M. Ma, and J.-M. Wang (2008), Turbulent flux transfer over bare soil surfaces: Characteristics and parameterization, *J. Appl. Meteorol. Climatol.*, *47*, 276–290, doi:10.1175/2007JAMC1547.1.

Yang, K., Y. Chen, and J. Qin (2009a), Some practical notes on the land surface modeling in the Tibetan Plateau, *Hydrol. Earth Syst. Sci.*, *13*(5), 687–701, doi:10.5194/hess-13-687-2009.

Yang, K., T. Koike, I. Kaihotsu, and J. Qin (2009b), Validation of a dual-pass microwave land data assimilation system for estimating surface soil moisture in semiarid regions, *J. Hydrometeorol.*, *10*(3), 780–793, doi:10.1175/2008JHM1065.1.

Zaitchik, B. F., M. Rodell, and F. Olivera (2010), Evaluation of the Global Land Data Assimilation System using global river discharge data and a source to sink routing scheme, *Water Resour. Res.*, *46*, W06507, doi:10.1029/2009WR007811.

Zhang, J., W.-C. Wang, and J. Wei (2008), Assessing land-atmosphere coupling using soil moisture from the Global Land Data Assimilation System and observational precipitation, *J. Geophys. Res.*, *113*, D17119, doi:10.1029/2008JD009807.

Zilitinkevich, S. S. (1995), Non-local turbulent transport: Pollution dispersion aspects of coherent structure of convective flows, in *Air Pollution III*, vol. I, *Air Pollution Theory and Simulation*, edited by H. Power, N. Moussiopoulos, and C. A. Brebbia, pp. 53–60, Wessex Inst. of Technol., Southampton, U. K.

T. Koike, Department of Civil Engineering, University of Tokyo, 7-3-1 Hongo, Bunkyo-ku, Tokyo 113-8656, Japan.

W. Li, Fengman Hydropower Plant, Jilin 132108, China.

A. Wang, Nansen-Zhu International Research Center, Institute of Atmospheric Physics, Chinese Academy of Sciences, Beijing 100029, China.

F. Wang and H. Zhou, Institute of Water Resources and Flood Control, Faculty of Infrastructure Engineering, Dalian University of Technology, Dalian 116024, China. (wangfuxings@gmail.com)

L. Wang and K. Yang, Institute of Tibetan Plateau Research, Chinese Academy of Sciences, Beijing 100085, China.